ELECTROCHEMICAL COMPARISON AND DEPOSITION OF LITHIUM AND POTASSIUM FROM PHOSPHONIUM- AND AMMONIUM-TFSI IONIC LIQUIDS

A Thesis
Presented to
The Academic Faculty

By

Jose A. Vega

In Partial Fulfillment
Of the Requirements for the Degree
Master of Science in Chemical and Biomolecular Engineering

Georgia Institute of Technology

May 2009

Electrochemical Comparison and Deposition of Lithium and Potassium from Phosphonium- and Ammonium-TFSI Ionic Liquids

Approved by:

Dr. Paul A. Kohl
School of Chemical & Biomolecular Engineering
Georgia Institute of Technology

Dr. Tom Fuller
School of Chemical & Biomolecular Engineering
Georgia Institute of Technology

Dr. Jiri Janata
School of Chemistry & Biochemistry
Georgia Institute of Technology

Date Approved: November 24, 2008

For Dad

ACKNOWLEGMENTS

My gratitude to Dr. Paul Kohl who guided me throughout this project. I wish to recognize Dr. Junfeng Zhou's contribution in the synthesis of the salts used in this work.

To my family, their love and support made this work possible.

TABLE OF CONTENTS

LIST OF TABLES

LIST OF FIGURES

LIST OF ABBREVIATIONS & SYMBOLS

ε_o – Permittivity of Space

ε_r – Relative Dielectric Constant

η - Viscosity

σ - Conductivity

ρ - Density

C – Molar Concentration

Cc - Cobalticinium

CV – Cyclic Voltammetry

DSC – Direct Scanning Calorimeter

FTIR – Fourier Transform Infrared

IL – Ionic Liquid

K – Potassium

Mg - Magnesium

MP – Melting Point

MW – Molecular Weight

NMR – Nuclear Magnetic Resonance

Li – Lithium

q – Ion Charge Magnitude

$Quat^+$ - Quaternary Cation

r – Distance

S.P. – Switching Potential

$TFSI^-$ - bistrifluoromethanesulfonimide

V - Volts

W - Tungsten

SUMMARY

In this work, ionic liquids (ILs) were investigated for use as battery electrolytes. The ILs were synthesized from quaternary ammonium and phosphonium salts and $TFSI^-$. A dendrite free lithium metal anode was demonstrated by deposition of a lithium-potassium alloy.

Several phosphonium ILs were synthesized using the $TFSI^-$ and PF_6^- anions until a room temperature IL was obtained. The smaller size, highly symmetric PF_6^- anion yielded high melting point salts, while $TFSI^-$ yielded much lower melting point ILs. When a room temperature IL, $Bu_3HexP^+TFSI^-$, was obtained the analogous ammonium IL, $Bu_3HexP^+TFSI^-$, was synthesized and compared. The phosphonium-based ionic liquid showed improved stability and physical properties compared to the analogous ammonium-based IL. The phosphonium-based IL had higher conductivity, 0.43 mS/cm, than the ammonium-based IL, 0.28 mS/cm. The addition of LiTFSI to both ILs led to a decrease in conductivity and increase in viscosity. The lower viscosity and higher stability of the phosphonium-based IL led to higher current density and stability for electrodeposited lithium metal. IL reduction interfered with lithium deposition reflecting lower coulombic efficiencies and giving the appearance of an unstable lithium couple. An optimum deposition potential was found which was bounded by the electrochemical stability of each IL. The stability of lithium in the ILs increased at lower temperature due to slower reactivity with the IL. Addition of higher quantities of lithium ions caused a higher fraction of the cathodic current going to lithium deposition that was reoxidized.

The stability of lithium in the ILs increased at lower temperature due to slower reactivity with the IL.

The electrodeposition and reoxidation of potassium was also demonstrated. Deposition of a lithium-potassium alloy caused slight increases in the cathodic and anodic currents along with higher coulombic efficiencies. Also, it was found that a lithium-potassium alloy could be deposited at high current for long times without the occurrence of dendrites.

CHAPTER 1

INTRODUCTION

The need for high power and high energy density secondary energy storage devices for electronics applications has fueled a significant amount of research related to lithium-ion (Li-ion) batteries. This work has led to the widespread use of Li-ion cells with both organic liquid and polymer electrolytes. Their applications range from medical equipment to cameras, clocks, communication equipment, and many others. These batteries generally consist of a metal oxide cathode in which lithium is intercalated in the discharged state, an organic electrolyte that contains lithium ions and a carbon (graphite) anode with intercalated lithium in the charged state. A schematic of a lithium ion cell with current materials is shown in Figure 1.1.

Metal Oxide Cathode (Positive Terminal)	**Electrolyte (Lithium Salt in Solvent)**	**Carbon Anode (Negative Terminal)**
Examples: Discharged State: $LiMn_2O_4$, $LiCoO_2$, $LiFePO_4$ Charged State: $Li_{1-x}Mn_2O_4$, $Li_{1-x}CoO_2$	Salts: $LiPF_6$, $LiBF_4$, $LiClO_4$ Solvents: Ethylene, Propylene, Dimethyl Carbonate	Discharged State: Graphite Charged State: LiC_x

Figure 1.1 Schematic of current Li-ion battery

An example of the anode and cathode half cell reactions and overall reaction for the Li-ion cell are given in equations 1.1 to 1.3

$$Disch\arg e \leftrightarrow Ch\arg e$$

Anode: $$C + xLi^{+} + xe^{-} \leftrightarrow CLi_{x} \quad (1.1)$$

Cathode: $$LiCoO_{2} \leftrightarrow Li_{1-x}CoO_{2} + xLi^{+} + xe^{-} \quad (1.2)$$

Overall: $$LiCoO_{2} + C \leftrightarrow Li_{1-x}CoO_{2} + CLi_{x} \quad (1.3)$$

Lithium metal-based batteries are a desirable option because lithium has a low molecular weight, provides a more negative anode potential and has a higher theoretical capacity (3860 mAh/g) than its Li-intercalated carbon counterpart in current cells. However, there are significant technological issues to be addressed. First of all, safety is a great concern due to the volatility and flammability of the conventional non-aqueous organic electrolytes that are typically used in these systems. Second, electrodes using lithium metal are prone to forming dendrites when recharged [1,2,3]. This can lead to electrode shorting, high short circuit currents, heat generation and thermal runaway. In this work ILs are investigated as a possible conductive, non-volatile battery electrolyte. Also, a Li-K alloy is studied as a means of preventing dendrite growth in a lithium metal anode.

1.1 Ionic Liquids

Desirable properties for a battery electrolyte are low cost, nonflammabilty, low melting point, high ionic conductivity and large electrochemical stability window. Ionic liquids (ILs) have the potential to exhibit all of these critical electrolyte features and represent the leading candidate to replace current battery electrolytes. Although their conductivity is lower than current electrolytes, they do also offer high thermal and chemical stability, a wide electrochemical window and no considerable vapor pressure which makes them nonflammable and avoids drying out of the electrolyte. Their melting points can be below room temperature; these melts are called room temperature ILs. They are used as reaction media, so IL chemical reactivity is usually not desired. Figure 1.2 shows examples of typical organic cations (imidazolium, pyrrolidinium, quaternary ammonium) and inorganic anions ($AlCl_4^-$, PF_6^-,) used for the formation of ILs. The wide range of possibilities for cation-anion combinations makes possible tuning of the electrolyte properties for specific applications.

Combination of asymmetric organic cations with relatively large, low charge density inorganic anions can lead to the formation of room temperature ILs. On the other hand, small and symmetrical halide anions rarely form low melting point ILs. Room temperature ILs can be used for the electroplating of metals that would otherwise react with water, like sodium or lithium. Also, the wide electrochemical stability window of ILs allows for combination of lithium metal anodes with the conventional intercalation cathodes.

(A) (B) (C)

(D) (E) (F)

Figure 1.2 Chemical structures of (A) pyrrolidinium, (B) imidazolium, (C) quaternary ammonium, (D) tetrachloroaluminate, (E) hexafluorophosphate and (F) tetrafluoroborate

Much of the IL development for battery application has focused on materials that are liquid at room temperature [4,5]. A wide variety of imidazolium and quaternary ($Quat^+$) ammonium IL's have been studied for sodium [6,7] and lithium [5,8] electrodeposition. Imidazolium ILs offer a higher conductivity than the $Quat^+$-based ILs. It is believed that the aromatic ring has both less entanglement and assistance in distributing the charge across the molecule compared with the $Quat^+$ structure. However, $Quat^+$-based ILs are an alternative to imidazolium IL since they are easy to synthesize, have very good electrochemical stability and it is possible to prepare a wider variety of ILs with different properties [9,10,11].

Careful tuning of the $Quat^+$ structure alters the chemical and physical properties of the IL. Increasing the degree of asymmetry causes a decrease in the melting point due to a harder degree of crystallization [12]. In general, a smaller cation provides higher conductivity due to its higher mobility in the electrolyte. Introduction of higher electron releasing groups (longer alkyl chains) raises the electron density and makes the molecule more difficult to reduce, therefore enhancing the electrochemical stability of the $Quat^+$. Longer alkyl chains lower the electrostatic interaction between the cation and its counter anion due to a greater distance between ion center and lower charge density; this allows for a more facile phase transition, thus lowering the melting point. However, the longer alkyl chains increase the IL viscosity due to the added weight and a higher probability of entanglement. Alkyl groups with high packing density, like isoalkyl groups, have also shown to increase the viscosity due to a higher degree of entanglement. Introduction of methyl alkoxyl groups lowers the melting point and increases the conductivity. Although the effect of introducing the alkoxyl group is not completely understood, it is believed that electron donation from the alkoxyl group reduces the positive charge on the cationic center, reducing the electrostatic interactions.

Different properties of the IL can also be tuned by use of different anions. Large anions generally lower electrostatic interactions due to a decrease in the charge density and increase the intrinsic conductivity of the IL. Hydrophobic/hydrophilic properties can be adjusted by using different anions which controls the solubility of molecules in the IL. Two of the most studied IL anions for lithium and sodium deposition are chloroaluminate ($AlCl_4^-$) and bistrifluoromethanesulfonimide ($TFSI^-$). Chloroaluminate based ILs are formed via an acid-base reaction between an organic halide $Quat^+$ and $AlCl_3$ (Equation

1.4). This family of ILs also requires the presence of an additive, such as thionyl chloride or hydrochloric acid, to enable metal plating. It has been proposed that the additive decreases the degree of dissociation of the metal ion and its counterion by coordinating with the anion, giving greater freedom to the metal ion and making it available for electroreduction [7]. An excess of $AlCl_3$ is added in order to create an acidic IL containing $Al_2Cl_7^-$ (Equation 1.5) which can be neutralized by addition of NaCl or LiCl (Equation 1.6), this provides the source of metal ions for electrodeposition to the metallic state. Excess chloride is normally added to buffer the IL and compensate for acidity changes near the electrode.

$$Quat^+Cl^- + AlCl_3 \rightarrow Quat^+ + AlCl_4^- \quad (1.4)$$

$$AlCl_4^- + AlCl_3 \rightarrow Al_2Cl_7^- \quad (1.5)$$

$$Al_2Cl_7^- + NaCl \rightarrow NaAlCl_4 + AlCl_4^- \quad (1.6)$$

On the other hand, $TFSI^-$ based ILs are formed via ion exchange between the organic halide $Quat^+$ and LiTFSI (Equation 1.7). Unlike the chloroaluminate ILs, TFSI-based ILs do not require the presence of an additive to enable metal deposition. Simple dissolution of the metal-TFSI salt in the IL provides the source of metal ions for electrodeposition.

$$Quat^+Cl^- + LiTFSI \rightarrow Quat^+TFSI^- + LiCl \quad (1.7)$$

The room temperature conductivity of current ionic liquids varies depending on the constituent ions. The highest conductivities are normally obtained from imidazolium-based IL. The IL ethylmethylimidazolium BF_4 has a conductivity of 14mS/cm [13]. ILs based on quaternary, pyrrolidinium, piperidinium and pyridinium cations are characterized by much lower conductivities. The conductivity of quaternary-based ILs depends on the nature and size of the substituents and the symmetry of the ions [12]. In general, smaller substituents have less entanglement and induce higher mobility of the ions. Large, asymmetrical anions generally induce higher conductivities.

There are several other factors that will influence the conductivity of the IL. Viscosity clearly has an effect by limiting the movement of charge carriers through out the IL. In general, a higher number of charge carriers per unit volume will increase the conductivity of the electrolyte. However, this effect is challenging to quantify in ILs since the system is composed completely of ions. If ions of opposite charge are close enough to form a more stable aggregate, they will form a lower charge or neutral species which will carry less or no charge. The thermal energy of the constituent ions will affect their mobility and compete with the electrical attraction energy, affecting the ability to carry charge. The charge in an IL will be transported by the individual constituent ions as well as their charged combinations. The relative contribution of each species is normally associated to the ion individual diffusion coefficient.

ILs should be resistant to electrochemical reduction and oxidation within the electrode potential limits of their application. For Li-ion cells electrochemical windows of 4V or greater are preferred, allowing for performance stability during both the charge and discharge state. Electrochemical windows vary depending on the cation and anion

used. Halide anions (like Cl^- or Br^-) undergo oxidation at relatively low potentials and are responsible for narrow stability windows (<3V). On the contrary, larger anions such as $TFSI^-$ are oxidized at high anodic potentials, broadening the stability window. Quaternary cations are characterized by relatively large reduction potentials and normally provide an enhanced stability window when coupled with an adequate anion (>4V).

Although ammonium ILs have been widely studied, few reports can be found concerning phosphonium ILs [14,15]. These ILs are normally formed by nucleophilic (S_N2) addition of tertiary phosphines to haloalkanes (Equation 1.8).

$$R_3P + R'X \rightarrow R'R_3P^+X^- \qquad (1.8)$$

The phosphonium halide can also be converted to other anions, as shown in Equation 1.7, to enhance the stability window. Applications under study for this new family of ILs include supercapacitors[16], catalysis[17] and solar cells[18], between others. However, most of the current phosphonium ILs are based on relatively large cations mostly derived from trihexylphosphine. These ILs tend to have a high viscosity due to their large molecular weights and long alkyl chains. Therefore, it is desired to develop lower viscosity phosphonium ILs since viscosity has a significant effect on the electrolyte ionic conductivity, solute mass transfer, mixing, solubility and even equipment design.

Phosphonium ILs are interesting because they provide higher conductivity and electrochemical stability than their ammonium counterparts, along with higher thermal stability [19]. As a consequence, these ILs should provide an improved performance in the

electrochemical deposition and reoxidation of metals. Also, the feasibility of lithium electrodeposition and reoxidation from phosphonium ILs has recently been demonstrated [20]. Therefore, it is of interest to investigate the electrochemical aspects of this new family of ILs and their response to different experimental conditions to determine their potential as practical secondary lithium battery electrolytes.

Figure 1.3 A-E show the structures of the cations synthesized during this study and Figure 1.3F shows the $TFSI^-$ anion. The synthesis yielded ILs that were mostly solid at room temperature. However, $Bu_3HexP^+TFSI^-$ (Figure 1.3D) and $Bu_3HexN^+TFSI^-$ (Figure 1.3E) were liquid at room temperature and, were studied in more detail as electrolytes for Li-ion cells. Their equivalent chemical structure will allow for a fair comparison between quaternary phosphonium and ammonium based electrolytes for Li cells. The counter anion used in this investigation ($TFSI^-$) was chosen due to its high electrochemical stability. Both ILs were studied via cyclic voltammetry under a variety of conditions which include: different switching potentials, temperatures and Li^+ concentrations. The effect of the different conditions on the coulombic efficiency for the reoxidation of the deposited metal is reported.

(A) (B) (C)

(D) (E)

(F)

Figure 1.3 Structures of cations synthesized during this study (A-E) and anion coupled with the cations (F)

1.2 Lithium metal anode

Current lithium ion and lithium polymer batteries are limited by the carbon intercalation anode, which has a significantly lower theoretical capacity than a metallic lithium anode. Therefore, a solid lithium metal anode is of interest for high energy density batteries. However, lithium metal anodes form dendrites when recharged (Figure 1.4A) and cycled (Figure 1.4B) which causes serious safety issues. A physical separator can be introduced in the electrolyte to avoid contact between anode and cathode, but this will result in high cell impedance and low current densities. Also, increasing the spatial separation between the electrodes is not desirable as this also results in large resistive losses and low current densities. Therefore, the suppression of dendrites is essential for lithium secondary batteries with a metallic anode[21].

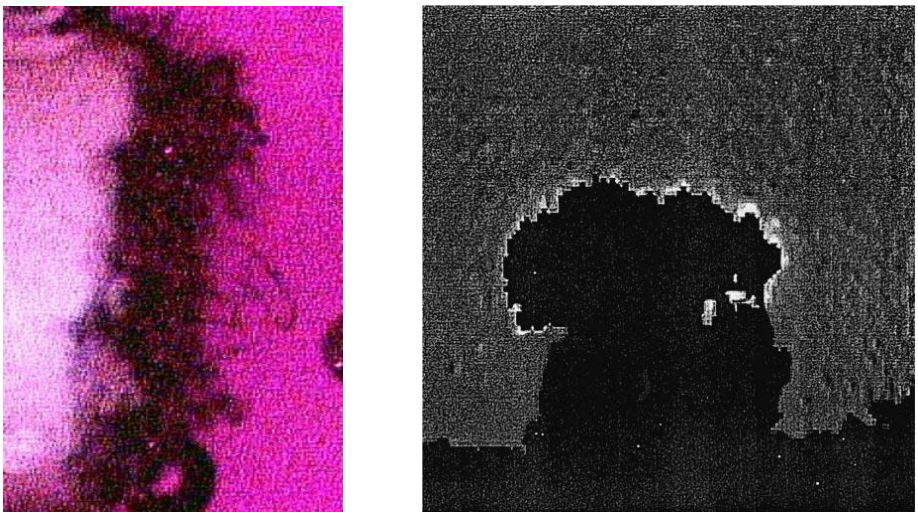

(A) (B)

Figure 1.4 Lithium only deposition from (A) ionic liquid electrolyte[22] and (B) polymer electrolyte[3]

Electrodeposition of other metals, such as zinc, tin and silver, also allows the formation of dendrites [23,24,25]. It is believed that dendrites form due to the different reaction rates of different crystal phases in certain metals. Metallic dendrites have been related to short circuits that cause electronic system failures. Dendrite suppression has been achieved by creating alloys consisting of the primary metal and a small amount of a secondary metal. For example, tin-lead is a reliable system for solderability [26]; and zinc-nickel is superior in corrosion resistance and thermal stability than zinc-only systems [27].

Lithium dendrite suppression has been achieved in chloroaluminate ionic liquids (ILs) by usage of a lithium-sodium alloy [22]; where application of a high reduction current for a long time showed no dendritic growth. The alloy deposition potential was more positive than for lithium only which in turn caused an increase in the coulombic efficiency. Also, lithium dendrite suppression was recently reported in an ethylene carbonate/diethylene carbonate electrolyte by usage of a lithium-magnesium alloy [28], where no dendrites were observed after continuous cycling of the electrode. Li-Mg alloy deposition also caused an increase in the coulombic efficiency.

In this work, a new lithium alloy was also investigated as a means to prevent dendrite formation during Li electrodeposition. Potassium was chosen as the secondary metal and KTFSI was used as the source of K^+ ions for deposition. Cyclic voltammetry was used to study the effect of the alloy on the coulombic efficiency. Visual observations were made to determine the presence or suppression of dendrites.

A lithium metal anode, IL electrolyte battery (Figure 1.5) will have several advantages over the conventional lithium ion batteries. The electrolyte is non-flammable and non-volatile, which would lead to safer operation and longer life. The absence of

dendrites will prevent electrode shorting which will also be an advance in safety and device life. The battery voltage will be higher and the anode mass will be smaller resulting in higher energy density.

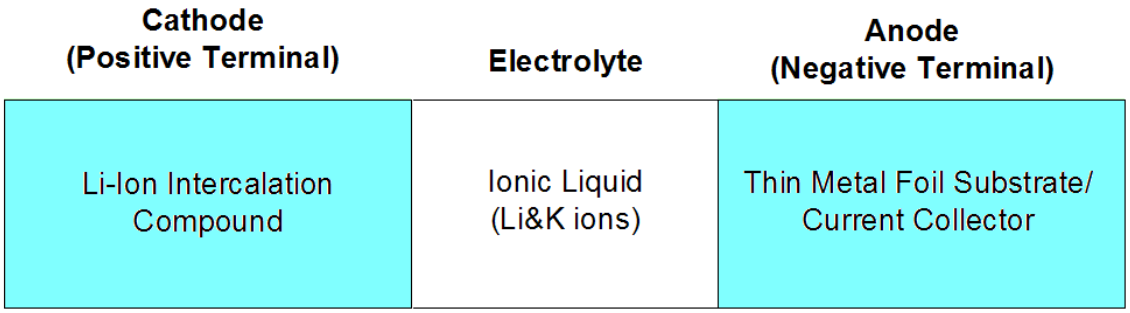

Figure 1.5 Proposed battery system

1.3 Literature Review

Ionic liquids are interesting because of several of their unique characteristics. Their popularity as green solvents arises from their negligible vapor pressure at room temperature which makes them both non-volatile and non-flammable. This allows the IL to be used as a reaction media and can be easily separated from volatile reactants and products. Earle et al. showed that some ILs can be evaporated and the recondensed at low pressures without decomposition [29]. Also, the vapor pressure and heat of vaporization of an imidazolium TFSI IL has been reported to be on the order of 10^{-2} Pa in the 184-244°C temperature range [30], which is negligible compared to organic electrolytes.

The useful electrochemical window of an ionic liquid is determined by the oxidation and reduction stability of the present ions. Modification of the alkyl groups in

the cation has been widely studied. Early work focused on the pyridinium cation, whose electrochemical window was limited to -1.16V vs. SCE by the reduction of the cation [31]. This stability window is to narrow for electrodeposition of lithium metal. Introduction of a dimethylamino group in the 1-alkylpyridinium caused an increase in the electrochemical window of approximately 700mV [32].

Wilkes et al synthesized several dialkylimidazolium cations and coupled them with chloroaluminate [33]. These ILs had similar electrochemical stabilities to ILs with pyridinium cations. These systems were able to solvate several compounds, including $CuCl_2$ and $TiCl_4$. Further improvements in the imidazolium cation stability were achieved by Gifford and Palmisano by replacing the hydrogen at the C-2 position with a methyl group, however this caused an increase in the viscosity [34].

The introduction of non-alkyl groups to quaternary and imidazolium cations has also been investigated. Replacement of $-CH_2C(CH_3)_3$ with $-CH_2Si(CH_3)_3$ in an imidazolium cation caused a decrease in the viscosity when coupled with BF_4^- and $TFSI^-$ anions [35]. It has been demonstrated that inclusion of an ether group in the cation lowers the melting point of the IL [36,37,38]. For example, cations containing an ether group can result in room temperature ILs when coupled with the TFSI anion [9,11,39]. Incorporation of a nitrile function to imidazolium cations has also been studied, having electrochemical windows of approximately 3V [40].

Emphasis has also been given to identifying new anions than form room temperature ILs with quaternary and imidazolium cations. One of the main targets has been asymmetric, hydrophobic and water stable molecules. Imidazolium cations have been combined with several anions, such as BF_4^-, PF_6^-, $CF_3SO_3^-$ and $TFSI^-$ [41,42].

Imidazolium/TFSI melts have very low melting points and large electrochemical stability windows [36]. Similarly, many Quat/TFSI systems having low melting points have also been reported [10,43]. Perfluoroalkyltrifluoroborate ($R_FBF_3^-$, where R_F = CF_3, C_2F_5, n-C_3F_7, or n-C_4F_9) anions have been coupled with a variety of cations by Zhou et al, several of which are liquid at room temperature [37,38,44].

The wide electrochemical window of ILs allows for the study of reduction and oxidation reactions. The deposition of metals that would otherwise react with water, like lithium or sodium, has been extensively studied in various ILs. Yu et al demonstrated sodium deposition from an imidazolium IL in a mercury drop electrode [45]. Later, Scordilis-Kelley et al demonstrated lithium and potassium deposition in a mercury drop electrode from an imidazolium IL [46]. It was demonstrated that the presence of protons promotes the reduction of lithium and enhances the stability of the plated metal [47,48]. Gray found that 6 Torr HCl partial pressure was necessary to observe sodium plating and stripping from a chloroaluminate IL [49]. Fuller et al reported that addition of $SOCl_2$ also enabled sodium and lithium deposition from chloroaluminate ILs [50].

Room temperature ILs have been investigated for use in a lithium battery. An imidazolium chloroaluminate IL was tested as the electrolyte for a Li-ion cell with a $LiCoO_2$ cathode. The cell exhibited a voltage of 3.45V and coulombic efficiencies around 90% [51]. Several quaternary ammonium cations coupled with the TFSI anion were examined as potential battery electrolytes [52,53]. An eutectic melt made of LiTFSI and acetamide was liquid at room temperature and provided a voltage of approximately 3V during charge and discharge [54]. The imidazolium cation has also been studied coupled with $TFSI^-$ and BF_4^- anions; the TFSI IL had better capacity stability after several cycles

than an ethylene carbonate/dimethyl carbonate electrolyte [55]. Quaternary ammonium cations with a cyano group proved feasible for lithium deposition and oxidation in a stainless steel electrode [56,57].

It is clear that a wide variety of cations and anions can be combined to form liquids at room temperature and their properties can be tuned to specific applications. Other than battery and electroplating applications, ILs have been used for organic reactions [58,59], biocatalytic transformations [60], proton exchange membranes [61], numerical displays [62], solar cells [63,64] and supercapacitors [16,65].

CHAPTER 2

EXPERIMENTAL

The synthesis of the ionic liquids was carried in a round bottom flask that was continuously purged with nitrogen. The reaction temperature was controlled by immersion in an oil bath. All starting materials used in the synthesis and characterization of the quaternary ammonium and phosphonium ILs are shown in Table 2.1. Unless noted, all materials were used as received.

Table 2.1 Chemicals and materials used throughout this work

Chemical	Purity	Supplier
Tri-n-butylphosphine	95%	Alfa-Aesar
Tri-n-butylamine	99%	Alfa-Aesar
1-bromohexane	99%	Alfa-Aesar
1-bromopentane	99%	Alfa-Aesar
1-bromobutane	98%	Alfa-Aesar
1-bromopropane	99%	Alfa-Aesar
LiTFSI	99%	Acros Organics
KTFSI		Wako Chemicals
Sodium hexafluorophosphate	98%	Alfa-Aesar
Chlorofrom-D	99.8%atom	Acros Organics
Ethyl Ether	99%	VWR
HPLC water	Low TOC	VWR
KCl solution in water		Fisher Scientific
Nitric Acid		VWR
Carbon activated		Fisher Scientific
Silver Nitrate	99%	VWR
Cobalticinium hexafluorophosphate	98%	Sigma-Aldrich
Tungsten Wire	99.95%	Alfa-Aesar
Platinum Wire	99.999%	Alfa-Aesar
Platinum Foil	99.99%	Alfa-Aesar
Silver Wire	99.9%	Alfa-Aesar

Synthesis of the $Bu_3HexP^+TFSI^-$ IL was accomplished by reaction of tri-n-butylphosphine with a 10% molar excess of 1-bromohexane. The reaction was carried out at 70°C for 7 days in a round-bottom flask and a quaternary phosphonium bromide was obtained. The remaining reactants were removed by washing the product several times with diethyl ether. Diethyl ether was chosen because of the high solubility of the reactants and limited solubility of the product, which facilitated extraction of the product. After the product was separated, it was dissolved in water. Activated carbon was added in order to remove the reaction by-products and system impurities. Filtration was used to remove the activated carbon following the purification steps. After a transparent product was obtained, suggesting a neat IL was obtained, anion exchange was carried out in aqueous solution by mixing the resulting quaternary phosphonium bromide with LiTFSI for one day to yield a phosphonium $Quat^+$ with the $TFSI^-$ anion. The reaction mechanism is summarized in Figure 2.1.

Figure 2.1 Synthesis route for $Bu_3HexP^+TFSI^-$ IL

The resulting hydrophobic phosphonium IL, $Bu_3HexP^+TFSI^-$, was purified by washing with high purity water. The organic IL and water phase were separated. Silver nitrate ($AgNO_3$) was added to the aqueous phase to test for residual bromide. The presence of a precipitate in the water phase indicated that bromide remained in the ionic liquid phase. If bromide was detected, the IL was washed with water again. When no residual bromide was detected, the sample was dried under vacuum at 70°C for 48 hours. Finally, the sample was stored in a dry nitrogen atmosphere glove box (Vacuum Atmospheres). The preparation and purification of other ILs was carried out in the same way except that the appropriate staring phosphine or amine was chosen, or the resulting halide $Quat^+$ was exchanged using $NaPF_6$.

The resulting products were characterized by FT-IR (Nicolet) and NMR (Varian Mercury Vx 400) spectroscopy. Density measurements were obtained by using a pre-calibrated picnomenter (2.03mL @ 25°C). Viscosity measurements were performed using a slow-flow viscometer (Cannon Instruments). Above room temperature melting points were measured using a differential scanning calorimeter (DSC, Seiko Instruments). The ramp rate for the heating cycle was 5˚C/min. Below room temperature melting points were determined by continuously monitoring the temperature with a thermocouple while the liquid was slowly cooled and observing when a liquid-solid phase change occurred. All experiments were performed in the glove box with a custom-built cell and an ISOTEMP 3016 (Fisher Scientific) for temperature control.

LiTFSI and KTFSI were recrystallized in HPLC water and dried under vacuum at 90˚C for two days before being placed in the glove box. Dissolution of LiTFSI in the IL

required stirring for 3 hours at room temperature. On the other hand, dissolution of KTFSI required overnight stirring at 100˚C.

Conductivity measurements were performed with a ThermoOrion conductivity meter and a custom-built probe with platinum plates set at a fixed distance apart and with the corners sealed in glass to prevent bending or movement of the plates. Calibration was performed with a KCl calibration solution (Fisher Scientific) before use in the glove box. After each use the probe was cleaned with hot nitric acid, rinsed with de-ionized water and dried in an oven.

An EG&G model 263A potentiostat was used to perform the electrochemical measurements inside the glove box. Working tungsten (W) electrodes were fabricated by sealing W wire (0.5mm diameter, $0.002cm^2$ area) in glass tubes. Prior to use, the electrode was cleaned with hot nitric acid, polished with 0.3μm alumina powder and thoroughly rinsed with de-ionized water. The counter electrode was a glass sealed platinum foil. After each use, it was cleaned with hot nitric acid, rinsed with de-ionized water and dried in an oven. The reference electrode was a silver wire. The electrodes were arranged in the three electrode setup showed in Figure 2.2. In all measurements, the three electrodes were positioned as close as possible to one another. IR compensation was performed for the IL tests. All cyclic voltammetry measurements were performed at a scan rate of 10mV/s. Cobalticinium (Cc) hexafluorophosphate in a concentration of 10mM was used as an internal reference electrode; all potentials are reported vs. the Cc/Cc^+ couple.

For the electrochemical experiments involving lithium, a flame test was performed to prove its presence in the electrode. The electrode containing the metal from

the electrochemical deposition was immersed in deionized water to dissolve the metal. A platinum wire was immersed in the metal-containing solution and placed into a blue flame.

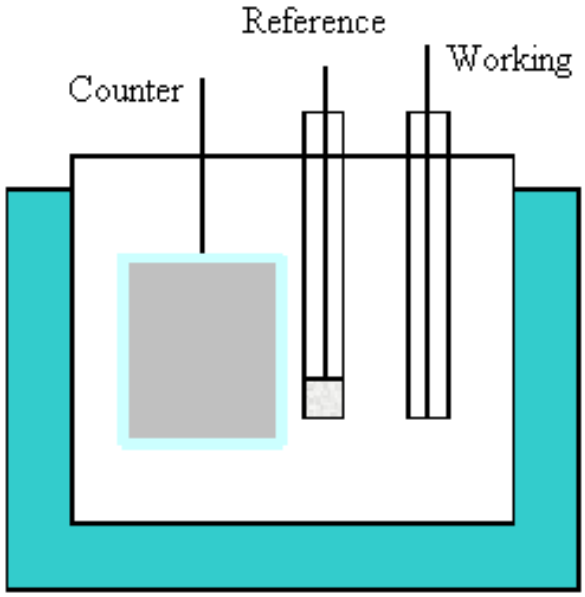

Figure 2.2 Three electrode cell schematic

CHAPTER 3

RESULTS

3.1 Synthesis and Characterization

In this study, it is of interest to compare the physical and electrochemical stability of room temperature phosphonium and ammonium ILs. A series of quaternary phosphonium-TFSI and phosphonium-PF_6 ILs were synthesized until a room temperature IL was obtained. The structures of the $TFSI^-$ salts made, $Bu_3ProP^+TFSI^-$, $Bu_4P^+TFSI^-$, $Bu_3PenP^+TFSI^-$ and $Bu_3HexP^+TFSI^-$, are shown in Figure 1.2A-D. The resulting products were characterized using FT-IR and ^1H NMR spectroscopy.

Figure 3.1.1 shows the FT-IR spectra for $Bu_3ProP^+TFSI^-$. The peaks present between approximately 2750 and 3000 cm^{-1}, a region free of peaks from the TFSI anion, are attributed to the symmetric and antisymmetric C-H stretching modes in the cation alkyl substituents. These peaks gradually increased in intensity with longer alkyl chain lengths in the other phosphonium ILs, because of the higher amount of the mentioned C-H vibrations. The peaks at lesser values (approximately <1500 cm^{-1}) are all attributed to different vibrations of the TFSI anion [66]. C-H bonds should also have bands close to 1460 cm^{-1} (asymmetric CH_2 bending) and at 850 cm^{-1} (CH_2 rocking); these are not clearly appreciated since they will be superimposed with the peaks assigned to TFSI vibration modes.

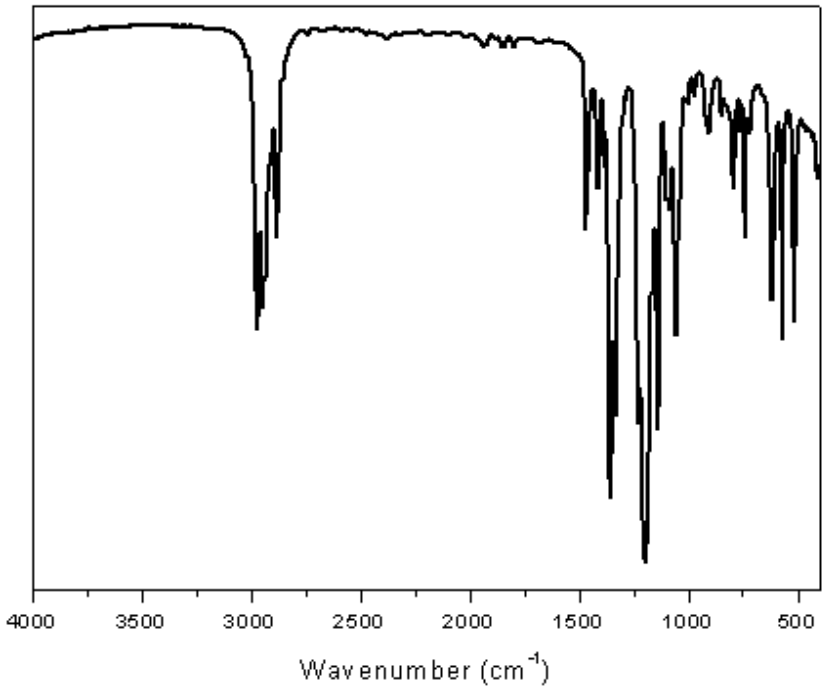

Figure 3.1.1 FT-IR spectra for $Bu_3ProP^+TFSI^-$

NMR spectroscopy was used to characterize the $Quat^+$ synthesized. Figure 3.1.2a shows the NMR spectra of the starting material, tri-n-butylphosphine, while Figure 3.1.2b shows the NMR spectra for $Bu_4P^+TFSI^-$. The peaks of the hydrogen atoms closest to the phosphonium center (identified as d in Figure 3.1.2) undergo the highest peak position shift in the obtained spectra. After alkylation, the electron density close to the cationic center undergoes the largest increase when another substituent is added and the electron spin of these hydrogen atoms will have the largest change, shifting the peak position. Position of other peaks is not appreciably changed due to a lower change in the electron density at positions farther from the cationic center.

(A)

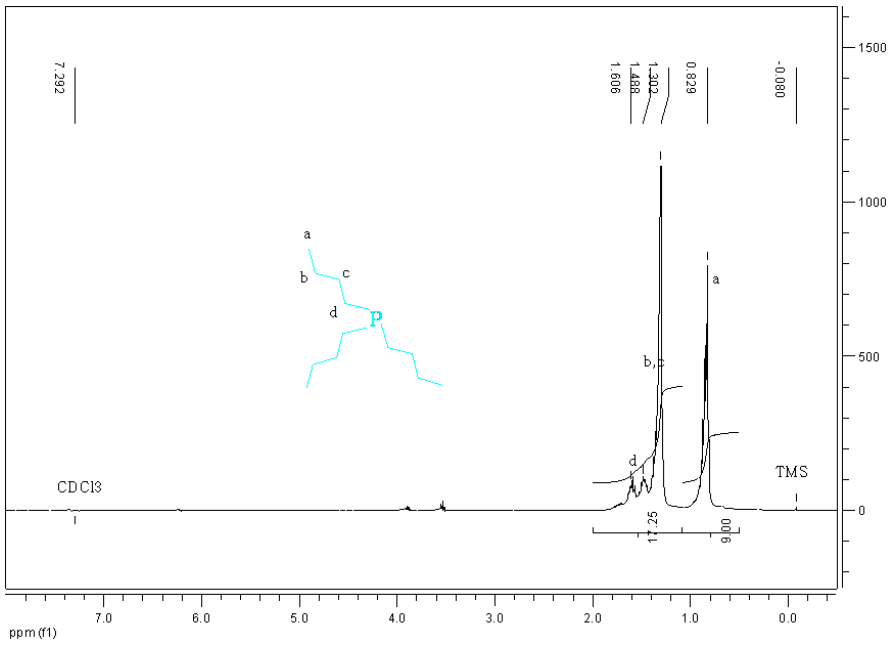

(B)

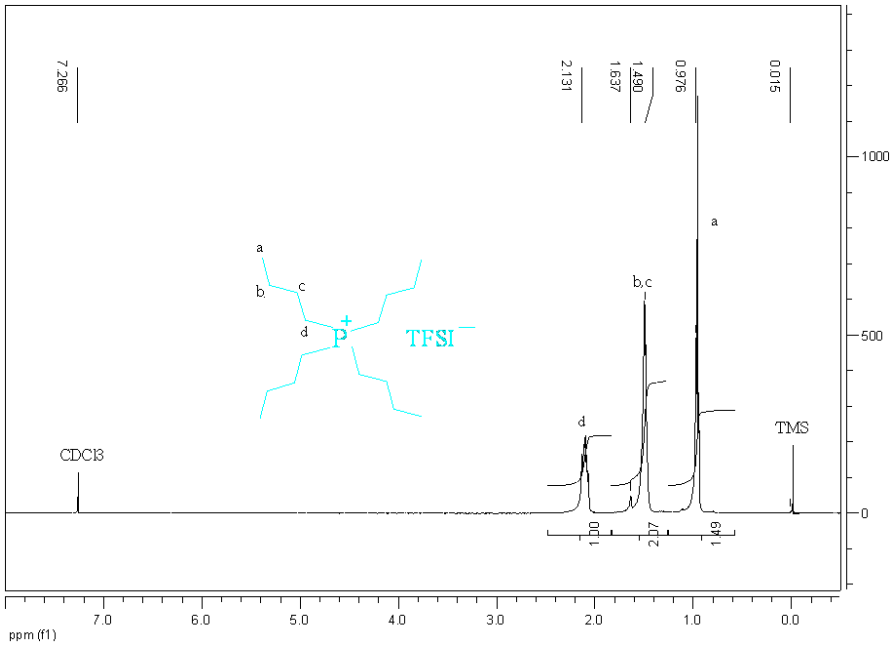

Figure 3.1.2 ^{1}H NMR spectra for (A) tri-n-butylphosphine and (B) $Bu_4P^+TFSI^-$

The ability of a quaternary ammonium IL to crystallize depends on the nature and shape of the substituents. Therefore, the melting point and viscosity will be affected by the size of the alkyl substituents and the overall symmetry of the ions [12]. Figure 3.1.3 shows the solid-liquid phase transition for the $Bu_3Pro^+TFSI^-$ IL, only one transition is observed at 65°C, the melting point of the IL. The melting points of the four phosphonium ILs are given in Table 3.1.1. Every solid-to-liquid phase transition temperature was confirmed by visual observation. In general, the melting point decreases as the size of the cation increases; with the exception of the completely symmetrical $Bu_4P^+TFSI^-$. These results are consistent with melting points observed in other ammonium-based ILs [12].

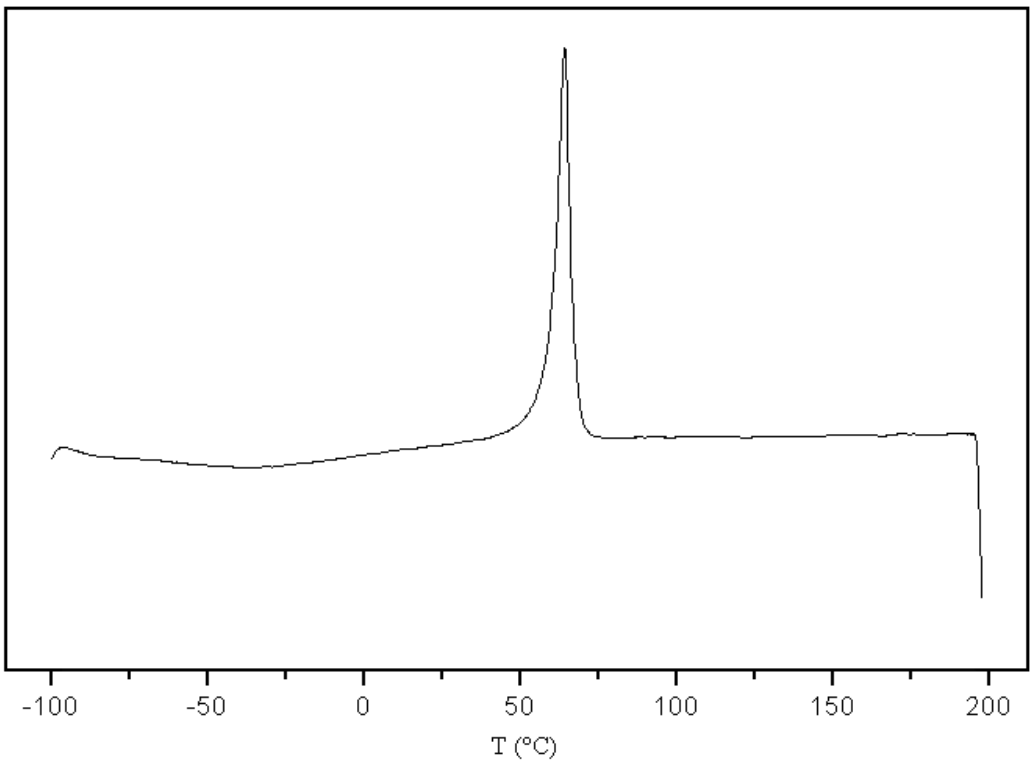

Figure 3.1.3 DSC curve for $Bu_3Pro^+TFSI^-$ IL

Table 3.1.1 Melting point of ILs synthesized

$Quat^+$	Melting Point (°C)	
	$TFSI^-$	PF_6^-
Bu_3Pro^+	65	225
Bu_4P^+	80	230
Bu_3PenP^+	34	180
Bu_3HexP^+	-18	145
Bu_3HexN^+	-6	168

The melting point of the $Quat^+PF_6^-$ salts was well above room temperature (Table 3.1.1). Nevertheless, these salts follow the same pattern of lower melting point as the size of the $Quat^+$ increases. However, the introduction of the smaller size, very symmetrical PF_6^- anion causes a considerable increase in the salt melting point.

The $Bu_3HexP^+TFSI^-$ IL was chosen for more detailed study because of its low melting point. The analogous ammonium IL, $Bu_3HexN^+TFSI^-$, was synthesized so that a direct comparison could be made between an ammonium and a phosphonium IL. The melting point of $Bu_3HexN^+TFSI^-$ was found to be -6°C (Table 3.1.1). During synthesis the reaction conditions were the same for both the phosphonium IL and ammonium IL. After completion of alkylation both products contained a yellow tint, signaling presence of by-products and impurities. The ammonium IL had a deeper yellow color. The quantity of product obtained was higher for the phosphonium-based IL, consistent with the faster kinetics of reaction observed with phosphines in comparison with amines [67]. The phosphonium-based IL was purified once with activated carbon to remove the impurities. In contrast, the ammonium-based IL was purified four times with activated carbon; which diminished the total yield of this reaction because of the separation

selectivity of activated carbon. The final ILs were transparent with the yellow tint being removed by the carbon treatment.

The physical properties of the two ILs are given in Table 3.1.2. Properties such as density, viscosity and ionic conductivity were measured at 25°C. The densities and viscosities are average values taken at room temperature using precalibrated flasks and viscometers. The molar concentration (C) was obtained by dividing the density by the molecular weight. The difference in viscosity between the two ILs is striking. The higher viscosity for the ammonium-based IL will certainly affect the diffusivity and mobility of ions within the IL, which will be higher in the phosphonium IL as evidenced in its higher intrinsic conductivity.

Table 3.1.2 Physical properties of $Bu_3HexP^+TFSI^-$ and $Bu_3HexN^+TFSI^-$

IL	MW	M.P. (°C)	ρ (g/mL)	C (mol/L)	η (cP)	σ (mS/cm)
$Bu_3HexP^+TFSI^-$	567.7	-18	1.18	2.08	261	0.43
$Bu_3HexN^+TFSI^-$	550.7	-6	1.19	2.16	397	0.28

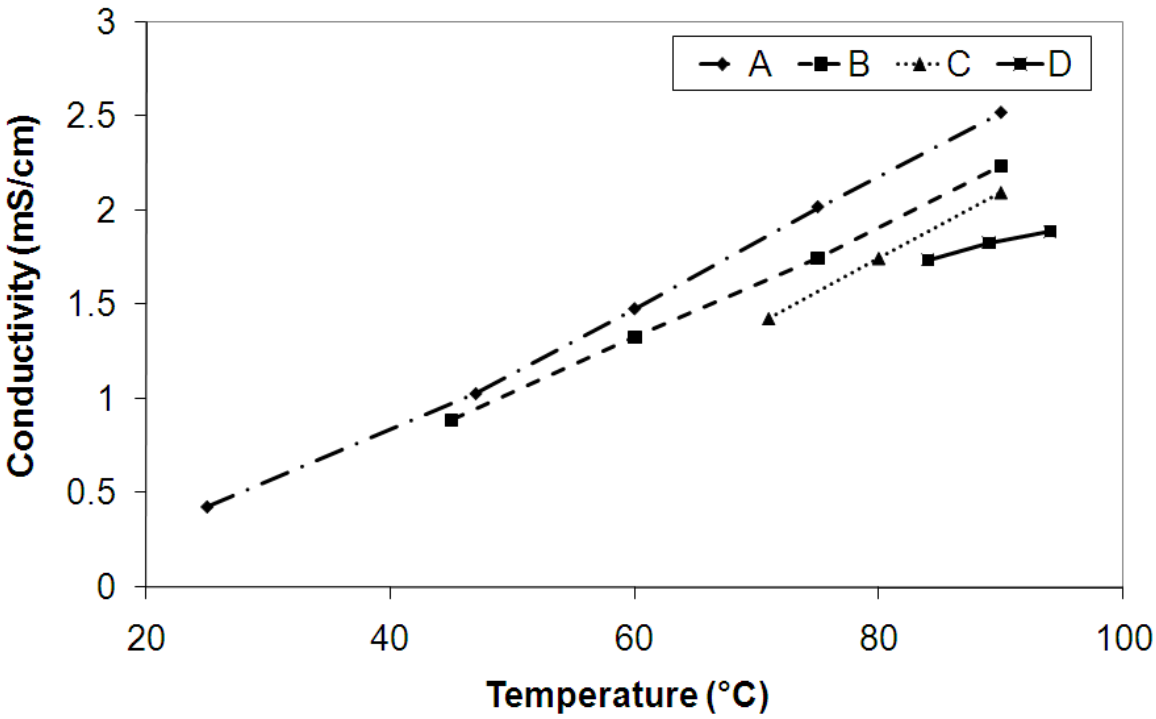

Figure 3.1.4 Conductivity vs. temperature for (A) $Bu_3HexP^+TFSI^-$, (B) $Bu_3PenP^+TFSI^-$, (C) $Bu_3ProP^+TFSI^-$ and (D) $Bu_4P^+TFSI^-$

Figure 3.1.4 shows the intrinsic ionic conductivity of the phosphonium ILs at different temperatures. Clearly, the conductivity offered by the IL increases as the melting point of the melt diminishes and the temperature increases. This shows that the conductivity of the melts (for this phosphonium chemical family) is closely tied to the viscosity. This result is consistent with the behavior observed for quaternary ammonium ILs [12].

3.2 Electrochemical stability

The electrochemical stability of $Bu_3HexP^+TFSI^-$ and $Bu_3HexN^+TFSI^-$ was evaluated in two ways. First, cyclic voltammetry (CV) was used to examine the stability of the neat IL. The cathodic limit of the IL is limited by the reduction of the $Quat^+$. Second, LiTFSI was added to each IL, and lithium was electrochemically deposited. The stability of the electrodeposited lithium in the IL was used as a probe of the stability of the IL to electroreduction. The stability of lithium metal is also of interest when considering these ILs as potential electrolytes for a lithium metal battery.

3.2.1 Stability of neat ILs

Figure 3.2.1.1 shows the voltammetric response for both ILs using a 0.5 mm diameter tungsten electrode. The electrochemical stability, as indicated by the onset potential for reduction of the ILs, is virtually the same at 25°C, with the onset at approximately -1.9V vs. Cc/Cc^+. The background current for the ammonium-based IL was slightly higher than for the phosphonium-based IL.

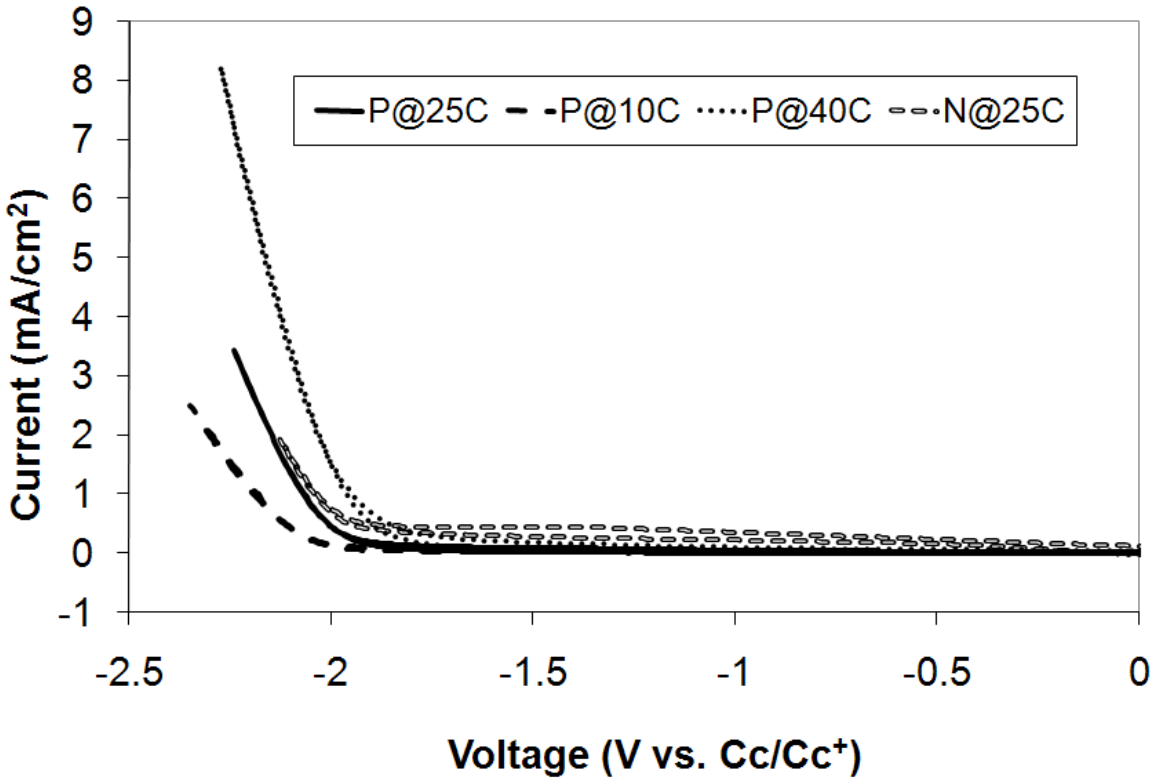

Figure 3.2.1.1 CV for neat $Bu_3HexP^+TFSI^-$ and $Bu_3HexN^+TFSI^-$

At higher temperature, the onset potential for IL reduction shifts to more positive values and at lower temperature the reduction of the IL is slower, as reflected in the shift in current to more negative potentials. This reflects the influence of thermal energy in the stability of the IL. The reduction of both ILs is an irreversible reaction, on the time scale of the CVs performed here. That is, no reoxidation current was observed on the positive-going scans. Thus, there is little difference in the electrochemical behavior of the two ILs, when measured for stability at a tungsten electrode.

3.2.2 Conductivity

Lithium ions were added to the IL via dissolution of LiTFSI to provide a source of lithium ions for electrodeposition and investigate the stability of lithium metal in the presence of the ILs. The conductivity of the ILs was measured as a function of the LiTFSI concentration at 25°C. The LiTFSI concentration was from 0.0 to 1.0 M for the ammonium-based IL and 0.0 to 1.5 M for the phosphonium IL. LiTFSI was not as soluble in the ammonium-based IL.

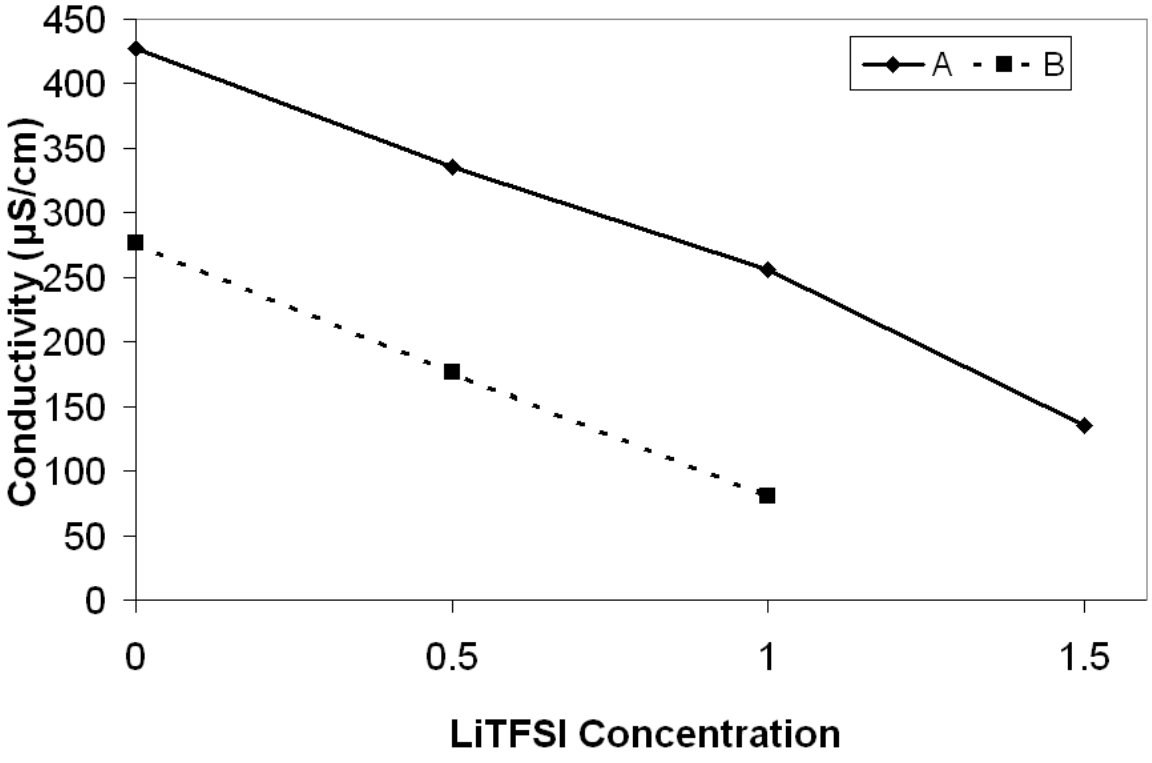

Figure 3.2.2.1 Ionic conductivity at 25°C vs. different Li^+ concentrations for (A) $Bu_3HexP^+TFSI^-$ and (B) $Bu_3HexN^+TFSI^-$

Figure 3.2.2.1 shows the drop in IL conductivity with LiTFSI concentration for the ammonium-based and phosphonium-based IL. The measurements were performed 2 times from ILs synthesized in different batches and the average value is reported. The difference between the values measured for one given IL was very small, 4%difference for phosphonium-based IL and 3% for ammonium-based IL. The rate of decrease in conductivity with LiTFSI is essentially the same for the two ILs.

The decrease in conductivity was accompanied by an increase in viscosity. The phosphonium-based IL had a viscosity of 261 cP in its neat form and nearly triple the viscosity (747 cP) with 1.5M LiTFSI. This follows the comparable increase in resistivity (essentially triple) over the same concentration range. The ammonium IL had a viscosity of 397 cP in its neat form and 1583 cP with 1M LiTFSI. Clearly, conductivity and viscosity are two closely related characteristics. This trend follows previous results with other ILs where the addition of small cations increased the resistivity [7]. This trend is different from solvent-solute systems where smaller ions normally provide higher conductivity.

3.2.3 Characterization of lithium electrodeposition

The electrochemical behavior of a tungsten electrode in the LiTFSI containing IL is quite different from the neat IL. Figure 3.2.3.1 shows the CV response for the phosphonium-based and ammonium-based ILs with 1M LiTFSI at 25°C. The switching potential for the CV scan was -2.1V. The magnitude of the reduction current at potentials negative of -1.8 V is greater than the background scans shown in Fig. 3.2.1.1 at the same

temperature. Further, a hysteresis in the reduction current and an oxidation peak is observed following the reduction process. Both these observations are consistent with the reduction and reoxidation of lithium metal [22]. The hysteresis in the reduction curves has been attributed to an overpotential for reduction when lithium is first deposited on a foreign surface (i.e. tungsten). The anodic peak is due to reoxidation of the lithium metal deposited during the reduction process. The reduction of lithium ions to lithium metal is superimposed on the small background reduction current due to impurities, as observed with the neat ILs in Fig. 3.2.1.1. The onset of the lithium ion reduction in Fig. 3.2.3.1 occurs at slightly more positive potential (e.g. -1.8 V) compared to Fig. 3.2.1.1.

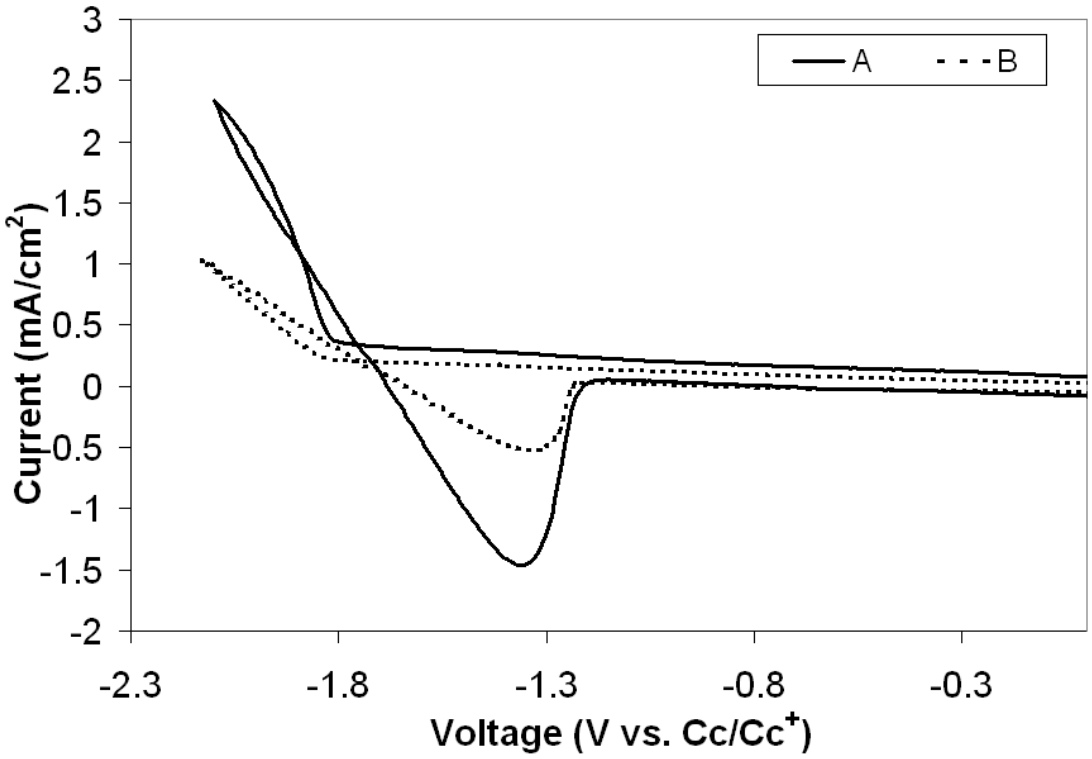

Figure 3.2.3.1 CV for (A) $Bu_3HexP^+TFSI^-$ and (B) $Bu_3HexN^+TFSI^-$ containing 1M LiTFSI at 25°C and switching potential of -2.1V

Flame tests were performed to verify for lithium electrodeposition in the working electrode. Immersion of the working electrode on de-ionized water caused evolution of bubbles, consistent with the reaction of lithium with water forming hydrogen gas. A platinum wire was immersed in the metal-containing solution and placed into a blue flame. Lithium produces a red flame which was clearly observed when the wire was exposed to the flame.

3.2.4 Effect of switching potential on lithium stability

The electrochemical response was studied in relation to the deposition potentials applied. Figure 3.2.4.1 shows the CV response for $Bu_3HexP^+TFSI^-$ with 1.5M LiTFSI at 25°C and various switching potentials in a tungsten electrode. Switching the potential to lower values causes an increase in cathodic and anodic currents. However, it causes decreases in the stability of deposited lithium.

Coulombic efficiencies are a practical method of investigating the stability of the lithium deposition and reoxidation process. Here, the coulombic efficiency is defined as the ratio of oxidation charge due to lithium stripping divided by the reduction charge. The coulombic efficiencies were calculated from the CV curves using two methods. First, the efficiencies were calculated using only cathodic and anodic currents. That is, the reduction charge includes the reduction of the impurities in the IL. The oxidation charge was obtained from the integral of the negative current, such as in Fig. 4. The inclusion of the background impurity current will give an overly pessimistic value of lithium stability. This is referred to as Method 1.

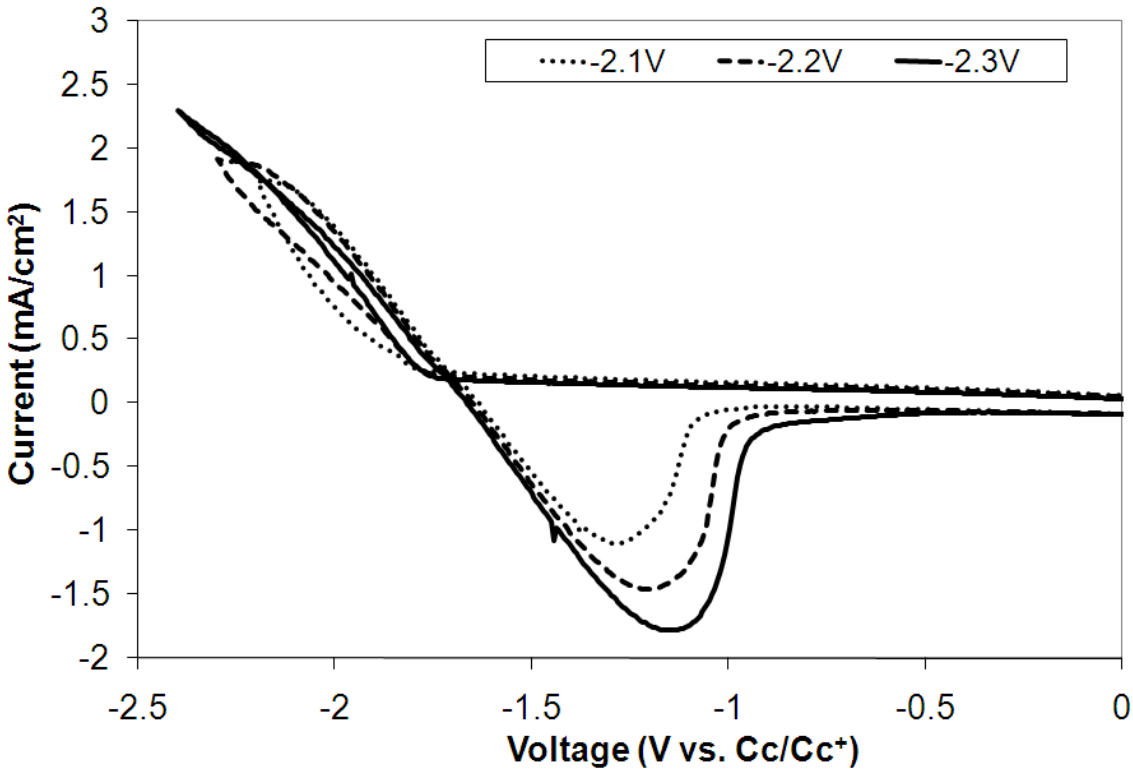

Figure 3.2.4.1 CV for $Bu_3HexP^+TFSI^-$ IL at 25°C, 1.5M LiTFSI and different switching potentials

Since the impurity current may not be present during battery operation, a second method was used to calculate the efficiencies which more closely resembles the true stability of lithium. The coulombic efficiency was calculated from the area under the cathodic and anodic current curves using the impurity background current as a baseline. That is, the near linear I-V curve at potential positive of -1.8 V was extrapolated to -2.1 V. This presumably would be the coulombic efficiency if the impurity were not present in the IL. This is referred to as Method 2.

Table 2 shows the coulombic efficiencies at different switching potentials for 1M LiTFSI in the ILs at 25°C using both calculation methods. The measurements were

performed 2 times and the highest value is reported. The coulombic efficiency of lithium reduction and reoxidation was slightly higher for the phosphonium IL than the ammonium IL. Method 2 probably provides a more accurate comparison of the two ILs because it compensates for a different level of background impurity. The most likely loss of coulombic efficiency is direct reduction of the IL and not Li^+ or direct reaction of the lithium with IL. In either of these cases, the more stable IL should yield higher coulombic efficiency. Fig. 3.2.1.1 shows that the IL is reduced at tungsten in this potential range. Other losses of coulombic efficiency include lithium dendrites falling off the electrode. These secondary loss mechanisms were hard to validate or quantify.

When the switching potential is made more negative (Table 3.2.4.1), the efficiency increases using Method 1 simply because the overall current becomes large compared to the background current. However, using Method 2, the coulombic efficiency decreases slightly at more negative potentials because the reduction of the IL (see Fig. 3.2.1.1) begins to become more appreciable. Recall that at potentials where the IL can be reduced, it has a substantial concentration advantage compared to the concentration of Li^+.

Based on higher coulombic efficiency for lithium (Table 3.2.4.1) and lower direct reduction current of the phosphonium-based IL (Fig. 3.2.1.1), it is reasonable to conclude that the phosphonium IL is electrochemically more stable at negative potentials than the analogous ammonium IL. Since the only difference between the two mixtures is the nitrogen vs. phosphorous portion of the ion, one is drawn to the slightly larger size of the phosphonium center and resulting lower charge density, i.e. lower nucleophilic attack.

The lower charge density may also be the origin of the lower viscosity and higher solubility of LiTSFI because there is somewhat less of the tendency for ion-pairing.

Table 3.2.4.1 Coulombic efficiencies for both ILs at 25°C with 1M LiTFSI concentration

	Efficiency (%)			
	Method 1		Method 2	
S.P. (V)	Bu_3HexP^+ $TFSI^-$	Bu_3HexN^+ $TFSI^-$	Bu_3HexP^+ $TFSI^-$	Bu_3HexN^+ $TFSI^-$
-1.9	11	-	77	-
-2	30	16	67	62
-2.1	45	32	63	56
-2.2	46	39	59	50

3.2.5 Effect of temperature on lithium stability

The electrochemical response as a function of temperature is of interest because it may give insight into the relative competition between lithium ion reduction and IL reduction, and it is of interest for potential battery applications. Figures 3.2.5.1A-B shows the CV response for 0.5M LiTFSI dissolved in the phosphonium-based and ammonium-based IL at different temperatures. The switching potential in each experiment was -2.1 V. The magnitude of the reduction and oxidation currents depends on temperature mainly because the viscosity and mobility of the ions is different. The change in temperature also had an effect on the coulombic efficiency of lithium. Table 3.2.5.1 shows the coulombic efficiencies for the phosphonium-based and ammonium-based IL with 0.5M LiTFSI at different temperatures and switching potentials using

Method 2 as the basis for calculation. In each case, the phosphonium-based IL was more stable than the corresponding ammonium-based IL. The highest efficiencies measured in the phosphonium-based IL were 84% and 35% for the ammonium-based IL, which occurred at 10°C. At high temperature, 40°C, the stability of lithium in the ILs decreased and a lower fraction of lithium metal was recovered. While this may be solely due to that fact that lithium ion reduction is more competitive with direct IL reduction at lower temperature (i.e. the rate of IL reduction decreases more with temperature than the rate of lithium ion reduction), the lower current density may also be a contributory factor because of secondary effects at high current (e.g. material falling off the electrode).

It is interesting to note that a mass-transfer limited current peak is observed only in the phosphonium-based IL, as shown in Fig. 3.2.5.1. This shows that Li^+ reduction is favored over IL reduction, which is consistent with the higher coulombic efficiency for lithium ion reduction (Table 3.2.5.1). That is, the mass transport limited condition can be reached for the phosphonium-based IL because a greater fraction of the current goes to Li^+ reduction (vs. IL reduction) before the onset of significant IL reduction.

Table 3.2.5.1 Coulombic efficiencies at different temperatures for Bu_3HexP^+ $TFSI^-$ and Bu_3HexN^+ $TFSI^-$ with 0.5M LiTFSI

	Efficiency (%)					
	Bu_3HexP^+ $TFSI^-$			Bu_3HexN^+ $TFSI^-$		
S.P. (V)	10°C	25°C	40°C	10°C	25°C	40°C
-1.9	84	74	67	-	-	-
-2	77	62	63	35	30	28
-2.1	66	60	48	29	23	24
-2.2	-	-	-	21	17	17

(A)

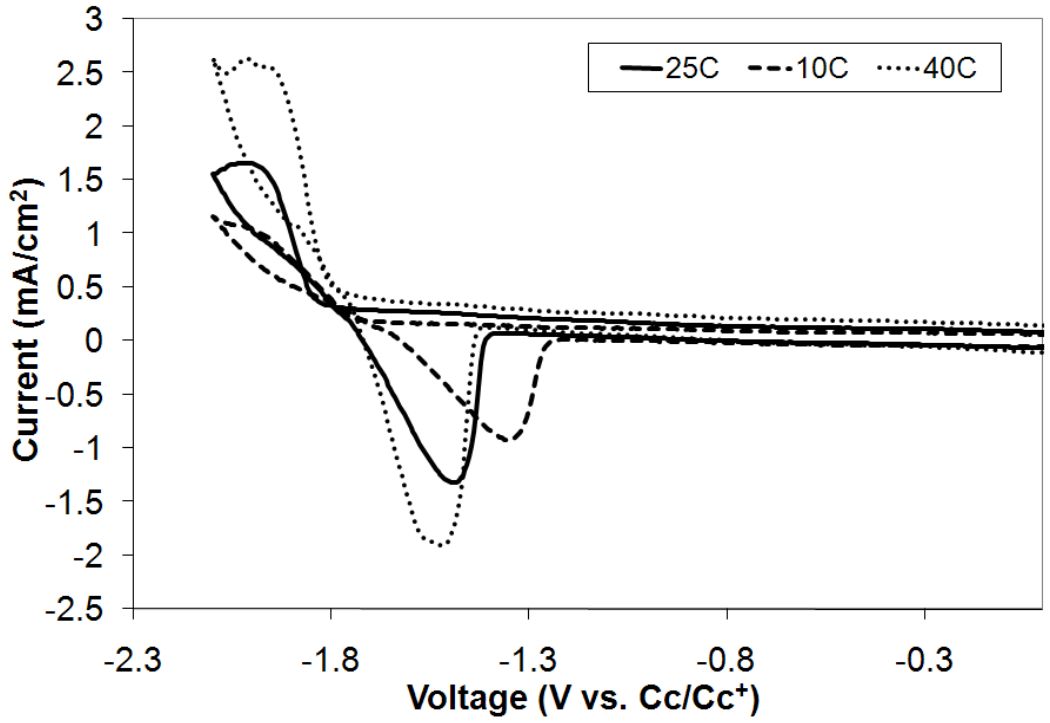

(B)

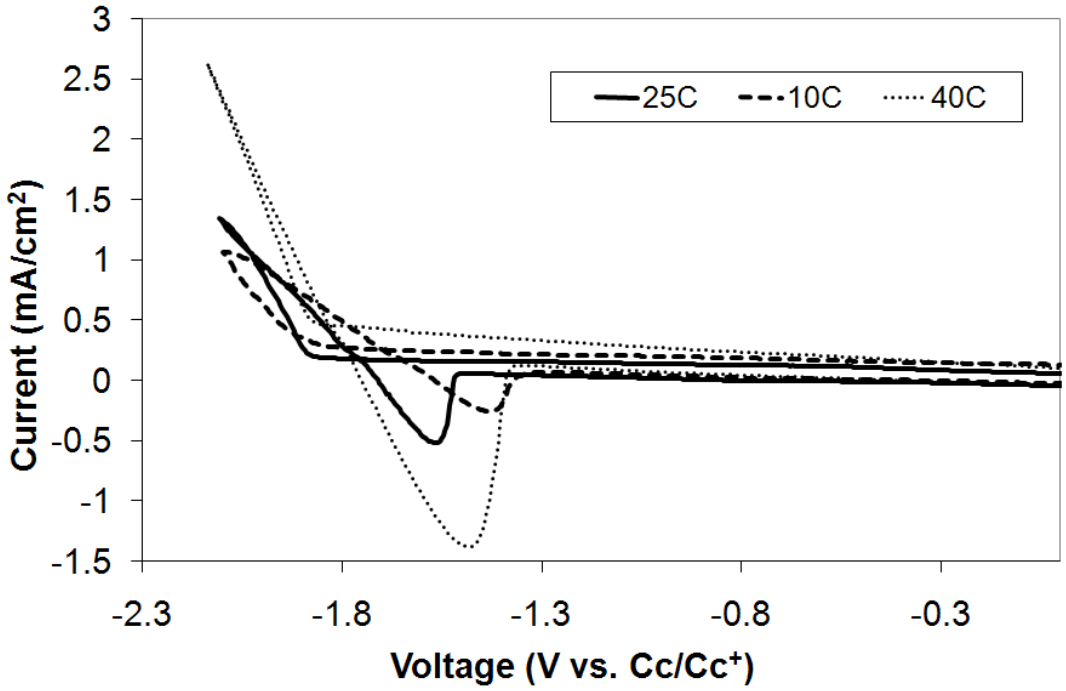

Figure 3.2.5.1. CV at different temperatures, 0.5M LiTFSI concentration and switching potential = -2.1V for (A) Bu_3HexP^+ $TFSI^-$ and (B) Bu_3HexN^+ $TFSI^-$

3.2.6 Effect of LiTFSI concentration on lithium stability

The electrochemical behavior of the electrode clearly differs as the LiTFSI concentration is gradually varied. Figure 3.2.6.1A shows three different LiTFSI concentrations (0.5M, 1.0M and 1.5M) in the phosphonium IL at 25°C. The switching potential for each scan was -2.1V. The cathodic and resulting reoxidation current increased when the Li^+ concentration was increased from 0.5M to 1.0M because there is a greater amount of Li^+ available for reduction. However, the current decreased upon further addition of LiTFSI due to the increase in viscosity and resulting decrease in diffusivity of Li^+, as shown by the conductivity decrease in Fig. 3.2.2.1. The same trend was observed in the ammonium-based IL, as shown in Figure 3.2.6.1B. An increase in the LiTFSI concentration from 0.5 to 1M caused a decrease in the cathodic current and resulting anodic peak current.

If the cathodic current at potentials negative of -1.9 V were a competition between the reduction of the IL and Li^+, then one would expect to see a difference in coulombic efficiency with LiTFSI concentration. Table 3.2.6.1 gives the coulombic efficiency in each IL as a function of the Li^+ concentration and switching potential using Method 2 as the basis for calculation. When the LiTFSI concentration was increased, the fraction of reduction current resulting in lithium metal available for reoxidation increased. The ammonium-based IL had a larger increase in efficiency with LiTFSI concentration because the IL reduction is more competitive (greater fraction going to IL reduction than Li^+ reduction) than for the phosphonium-based IL reduction.

(A)

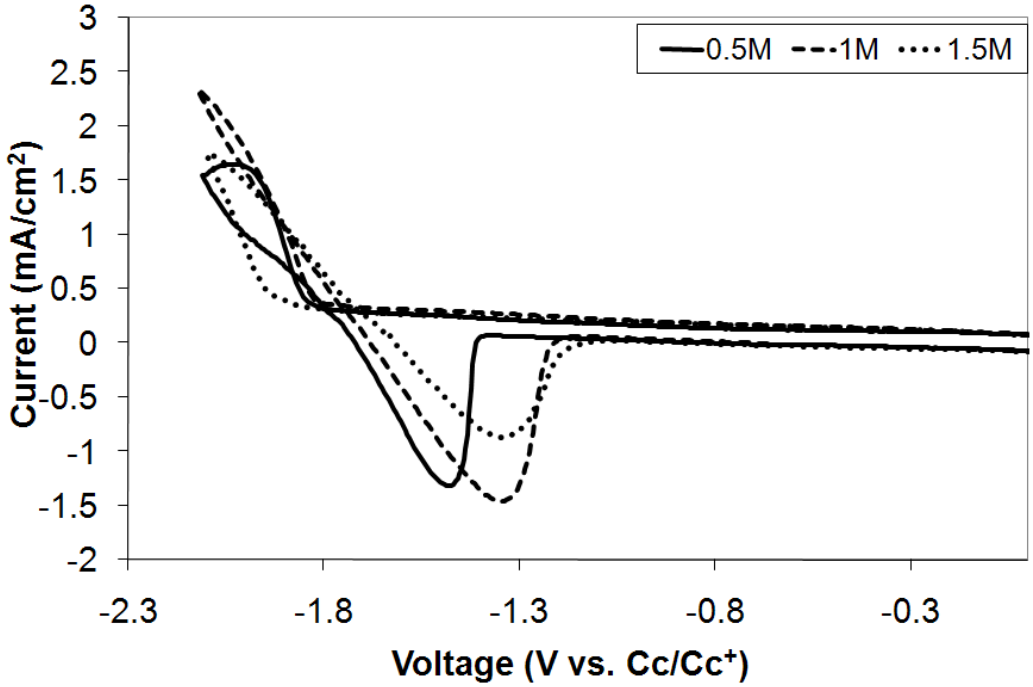

(B)

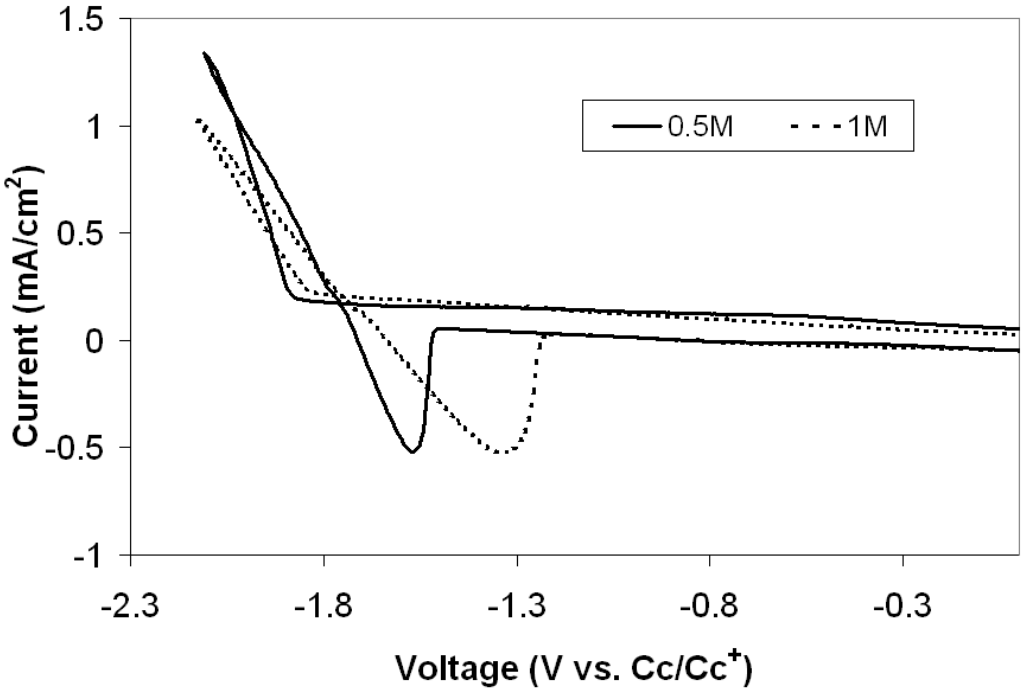

Figure 3.2.6.1 . CV at different concentrations, 25°C and switching potential = -2.1V for (A) Bu_3HexP^+ $TFSI^-$ and (B) Bu_3HexN^+ $TFSI^-$

Table 3.2.6.1. Coulombic efficiencies at different LiTFSI concentrations, 25°C for Bu_3HexP^+ $TFSI^-$ and Bu_3HexN^+ $TFSI^-$

	Efficiency (%)				
	Bu_3HexP^+ $TFSI^-$			Bu_3HexN^+ $TFSI^-$	
S.P.[a] (%)	0.5M	1M	1.5M	0.5M	1M
-1.9	74	77	80	-	-
-2	62	67	69	30	62
-2.1	60	63	67	23	56
-2.2	-	-	61	17	50

3.2.7 Characterization of potassium electrodeposition

In this work, potassium was chosen as the potential alloy metal due to the availability of KTFSI. The deposition of potassium has been previously reported on a mercury electrode by Scordillis-Kelley et al, although no deposition was observed on a tungsten electrode [46]. To demonstrate the feasibility of potassium electrodeposition and reoxidation on a W metal electrode, CVs were performed from the phosphonium IL containing KTFSI only. Figure 3.2.7.1 shows the CV response for the W electrode in a phosphonium IL melt with a KTFSI concentration of 0.25M, operating temperature of 25°C and switching potential of -2.3V. The onset for potassium ion only deposition (ca. -2.1 V) occurs at a more negative potential than the lithium ion reduction (ca. -1.8 V). The presence of an anodic peak following the scan to negative potentials shows that potassium metal was deposited during the reduction process. Nevertheless, the lower potential needed for potassium only deposition increases the probability of reaching the cathodic limit of the IL. Irreversible IL reduction can occur at a higher rate, disturbing

the potassium electrodeposition and consequently lowering the coulombic efficiency of the process.

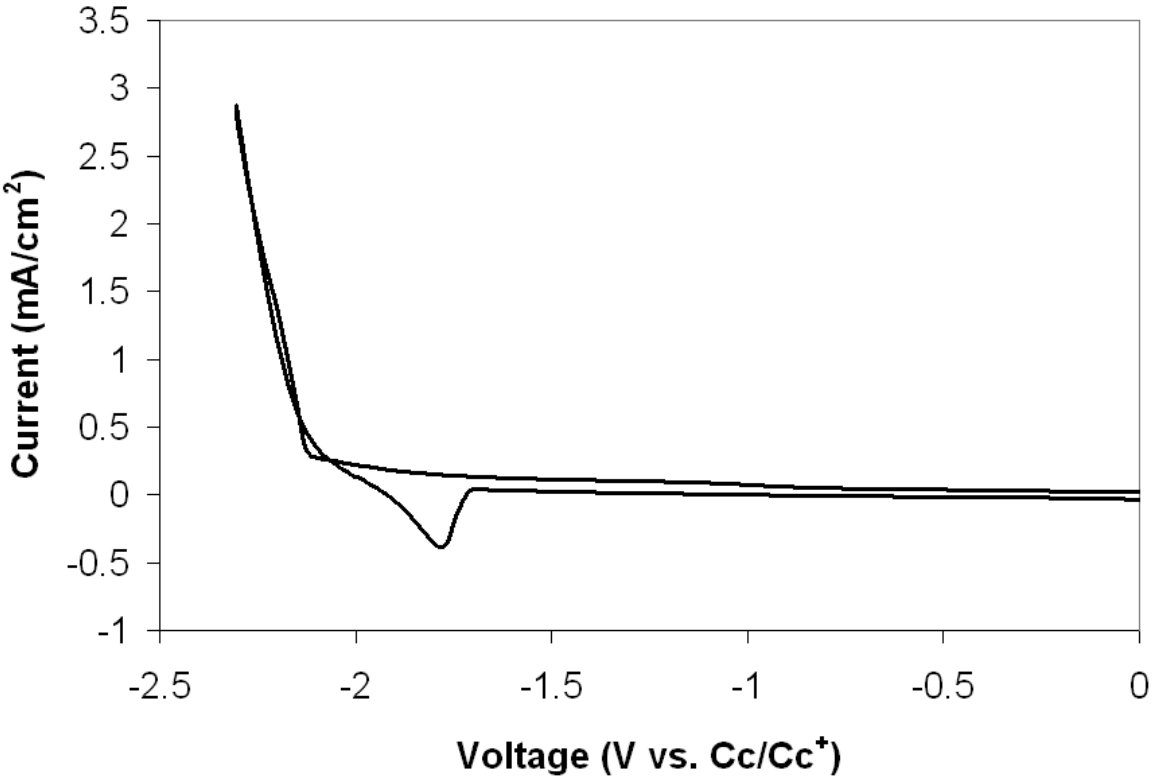

Figure 3.2.7.1 CV for Bu_3HexP^+ $TFSI^-$ IL at 25°C, 0.25M KTFSI and switching potential of -2.3V

3.2.8 Lithium-Potassium Electrodeposition

The codeposition of Li-K was investigated using a phosphonium-based IL with 0.075M KTFSI and 1.5M LiTFSI. The CV at a tungsten electrode with and without the addition of the 0.075M KTFSI is shown in Figure 3.2.8.1 at 25°C and switching potential of -2.3 V. The onset potential for alloy deposition was slightly more positive than for lithium or potassium alone. The standard potential for the deposition of an alloy can be different than that of the individual metals because of the energy of formation of the alloy. The shift in deposition potential to more positive values also resulted in an increase in the coulombic efficiency because the metal deposition competes more effectively with IL reduction at the more positive potentials, as shown in Table 3.2.8.1.

The increase in coulombic efficiency for the Li-K alloy may also have a contribution from an improved morphology of the deposited metal. That is, lithium is known to form dendrites, whereas the alloying metal can suppress dendrite formation. The working electrode was visually examined for dendrite growth. Particular care was taken during these observations because dendrites can be fragile. The electrode was maintained inside the IL during observation and the cell was not moved so as to minimize vibrations. The experiment consisted of constant reduction at 1.5 mA/cm^2 for 30 min. Dendrites were clearly observed on the electrode surface when the IL contained 1.5M LiTFSI only (no KTFSI present). The deposit was rough and had a needle-like morphology. When the electrode was gently shaken, a portion of the deposited metal could be seen falling off the surface of the electrode.

When KTFSI was added to the IL (1.5M LiTFSI and 0.075M KTFSI) and the experiment was repeated (1.5 mA/cm^2 for 30 min), no dendrites were observed under the same conditions using the same observation techniques. The surface of the electrode had a smooth and uniform deposit. When the experiment was extended to 60 min. deposition time, no dendritic growth was observed.

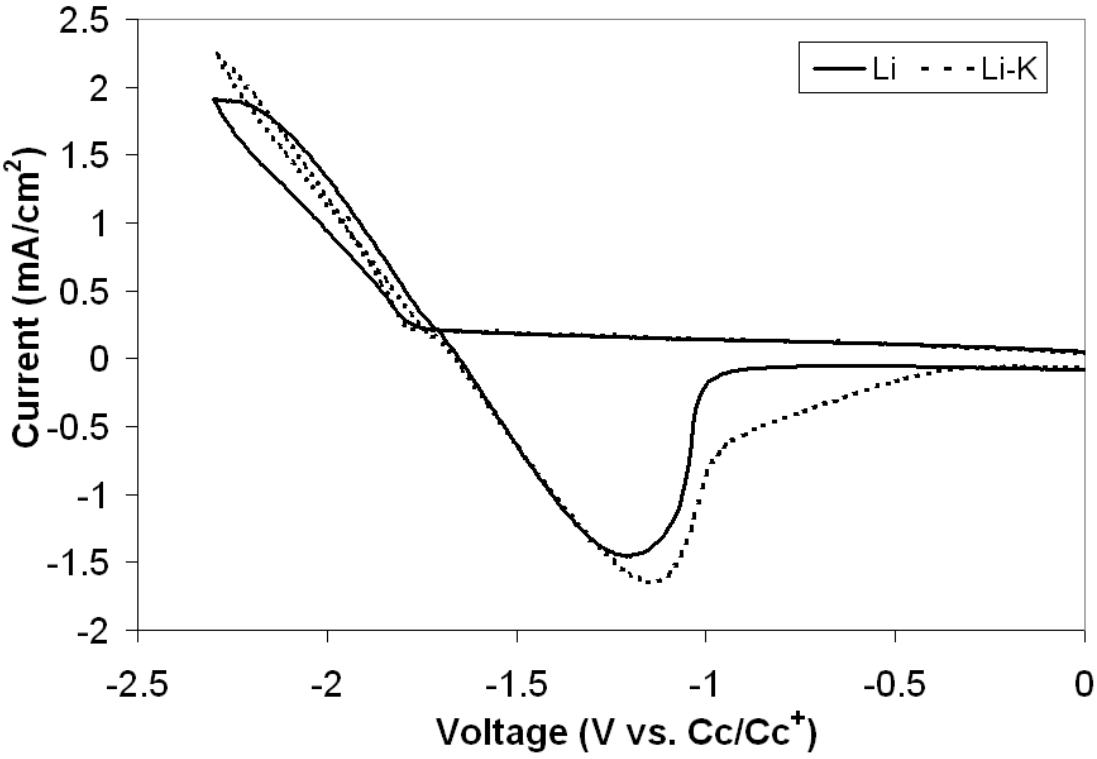

Figure 3.2.8.1 CV for Bu_3HexP^+ $TFSI^-$ IL with 1.5M LiTFSI & 0.075M KTFSI at 25°C and switching potential of -2.2V

Table 3.2.8.1 Coulombic efficiency for $Bu_3HexP^+TFSI^-$ IL at 25°C before and after addition of KTFSI

	Efficiency (%)	
S.P. (V)	1.5M LiTFSI	1.5MLiTFSI & 0.075M KTFSI
-2	69	80
-2.1	67	78
-2.2	61	70
-2.3	58	63

CHAPTER 4

DISCUSSION

A direct comparison of the physical and electrochemical properties between a quaternary ammonium-based and phosphonium-based IL showed several interesting differences. During synthesis and purification, the phosphonium-based IL was easier to synthesize and required fewer steps and shorter times to purify. There were significant differences in the physical properties of Bu_3HexP^+ $TFSI^-$ compared to Bu_3HexN^+ $TFSI^-$. Their electrochemical behavior in the presence of lithium varied according to the conditions it was exposed.

4.1 Conductivity

The concept of ion pairing is closely related to the overall conductivity of an electrolyte. When two ions of opposite charge are close together, the energy of electrical attraction may be greater than their thermal energy. These two ions could form a new entity stable enough to persist in solution. This new entity will have a net charge not previously present in the melt which will contribute to the conductivity, though less than it would if the constituent ions were in a free state. A very high degree of association can lead to the formation of zero net-charge entities which will make no contribution to the conductivity. However, the ion pair must be long-lived enough to be a recognizable entity and affect the kinetics of ion movement and charge transport.

The electrostatic interactions between the cation and anion of a salt can be described by using Coulomb's law (Equation 4.1.1), which states that the electrostatic force between two charges is directly proportional to the magnitude of each charge and inversely proportional to the square of the distances between the charges;

$$F = \frac{q_i q_j}{4\pi\varepsilon_o \varepsilon_r r_{ij}^2} \tag{4.1.1}$$

where q_i and q_j are the magnitude of the charges, r_{ij} is the distance between ions, ε_o the permittivity of space and ε_r the relative dielectric constant of the medium in which the charges are placed. According to this equation, when ions become larger the electrostatic interactions become weaker due to the greater distance between the ions (or charge) center.

The phosphonium-based IL has a significantly higher conductivity and lower viscosity compared to the ammonium-based IL over the entire range of LiTFSI concentration (Figure 3.2.2.1). Tsunashima et al. argued that this higher conductivity is due to lower electrostatic interaction between the phosphonium cation and the $TFSI^-$ anion, in comparison with the ammonium cation[19]. The larger radius of the phosphonium Quat implies greater distance between ions centers which diminishes electrostatic interactions according to Coulomb's law. This would lead to a higher mobility of the ions in solution, enabling them to more freely carry charge through the electrolyte. The subtitle difference is N^+ vs. P^+ size (and resulting difference in charge density) has a

dramatic effect on the ion-ion interactions. The weaker interactions of the phosphonium cation would result in the phase transition (melting) at lower temperature which will contribute to lower viscosities. In general, less anion-cation attraction would result in higher mobility of the ions in the IL and lower overall viscosity (Table 3.1.2).

The sensitivity to anion-cation interaction is also shown when lithium cations are added to the ILs. In a dilute, solvent-solute electrolyte, smaller ions generally have higher mobility so that replacing large ions with smaller ones results in higher conductivity. The ions are normally surrounded by solvent molecules and distributed over a large volume, which diminishes direct cation-anion interactions. Here, the addition of a relatively small number of lithium ions (e.g. 0.5M) leads to dramatic reduction in conductivity and increase in viscosity, although the potential number of ions (charge carriers) is increasing. This same effect of lower conductivity by replacing large ions with smaller ones has been observed in other ILs[7]. The ILs are very sensitive to electrostatic interactions of the ions since there is no solvent present to help distribute the charge over larger volumes and, therefore, the ions are in continuous direct contact. Although the mobility of a Li^+ would be higher than the $Quat^+$, the introduction of a small size, high charge density cation has a low contribution to the overall conductivity because of the degree of association (i.e. ion pairing) with the $TFSI^-$ anion. This is a particular concern in electrochemical devices based on small ions (e.g. Li^+) because they have the smallest mass (leading to high energy density devices) and have the highest mobility in the solvent-solute electrolytes.

4.2 Electrochemical Stability

The electrochemical stability of the IL $Quat^+$ and the deposited lithium metal is essential for battery operation. The reduction of the IL will not only interfere with metal ion deposition but also limit the lifetime of the electrolyte. The stability of the deposited lithium will depend on the stability of the $Quat^+$.

4.1.1 IL Electrochemical Stability

A wide electrochemical window is essential for many electrochemical applications. The cathodic limit of an IL is limited by the reduction of the IL cation. In the case of an ammonium $Quat^+$, reduction is thought to proceed through the production of a radical which can then undergo dimerization (Figure 4.1.1.1)

(A)

(B)

Radical Chain Reactions

Figure 4.1.1.1 Reduction of an ammonium $Quat^+$

Using mass spectroscopy, Lang et al. confirmed that ammonium $Quat^+$ reduction involves the loss of an alkyl group, with benzyl-substituted $Quats^+$ being less stable than alkyl substituted $Quats^+$ [68]. The substituents on the $Quat^+$ have a strong influence on the electrochemical stability. In general, electron donating groups raises the electron density on the charge center, making the molecule more difficult to reduce. A substituent which is a poor leaving group also contributes to higher electrochemical stability.

The analogous chemical structure of $Bu_3HexP^+TFSI^-$ and $Bu_3HexN^+TFSI^-$ will result in similar electrochemical stability of the cations at the same temperature (Figure 3.2.1.1), assuming that its reduction also involves the loss of an alkyl group. The introduction of more electron releasing groups (longer chain alkyl groups) to the $Quat^+$ could enhance the stability of the IL and contribute to higher coulombic efficiencies. However, longer alkyl chains will diminish the intrinsic conductivity of the IL due to lower mobility (bigger size) and higher probability of entanglement with adjacent molecules.

4.1.2 Lithium and Potassium Electrochemical Stability

The stability of the deposited metal, which was studied via coulombic efficiency, is generally related to the electrochemical stability of the IL cation. Howlett et al. reported coulombic efficiencies for lithium electrodeposition and reoxidation close to 99% from alkylpyrrolidinium TFSI-based ILs [69]. The cyclic structure of the alkylpyrrolidinum cations offers favorable cathodic stability which contributes to high cycling performance. However, much lower coulombic efficiencies (<50%) have been

observed from quaternary ammonium-TFSI based ILs [56]. Also, previous work has demonstrated that ILs lacking sufficient cathodic stability were not able to undergo electrodeposition and reoxidation of metals [47] or showed very poor performance [55].

The only difference between $Bu_3HexP^+TFSI^-$ and $Bu_3HexN^+TFSI^-$ is the phosphorous and ammonium ion. The higher cycling efficiency of the phosphonium-based IL points to its higher electrochemical stability compared to the ammonium-based IL. The bigger size of phosphorous (lower charge density) could lower the probability of direct nucleophilic attack, therefore contributing to higher efficiencies.

The faradaic processes at the working electrode are affected by the transport properties of the electrolyte, such as viscosity and ion mobility. In this study, the competition between IL reduction and metal deposition varied depending on the conditions. At higher temperatures the consumption of cathodic current by the irreversible reduction of the IL lowers both the coulombic efficiency of the lithium charge/discharge cycle and the lifetime of the electrolyte. In the case of an IL with very high cathodic stability the effect of temperature could be different. Higher temperatures will increase the mobility of small ions and lower the overall viscosity of the melt. The concentration of IL at the electrode surface during reduction remains essentially fixed and does not rely on diffusion to the same extent as metal ion transport relies on diffusion. Thus, lower viscosity and higher metal ion mobility will ease its movement to the electrode surface and lead to higher coulombic efficiencies. Therefore, the mobility of ions in solution will play a pivotal role in determining the cycleability and efficiency of lithium cells with IL electrolytes.

Alloy formation has several benefits for battery applications. First, the shift of the reduction potential to more positive values is an advantage because the metal reduction is better able to compete with electrolyte reduction resulting in higher cycling efficiency and lower self-discharge. The second advantage of alloy formation is the suppression of dendrites. The feasibility of potassium metal deposition on a tungsten electrode has been shown here for the first time (Figure 3.2.7.1). Dendrite suppression is an essential attribute for a lithium-metal anode in a battery, since dendrite formation can lead to electrode shorting, high short circuit currents, heat generation and thermal runaway.

CHAPTER 5

CONCLUSIONS AND FUTURE WORK

5.1 Conclusions

This work focused on obtaining a fair comparison between phosphonium and ammonium ILs for lithium electroplating. New ILs were synthesized and studied as potential electrolytes in lithium secondary batteries. The ILs were formed from quaternary ammonium and phosphonium salts and $TFSI^-$ and PF_6^- anions. The PF_6^- based salts were characterized by high melting points, while the $TFSI^-$ based salts had much lower melting points. $Bu_3HexP^+TFSI^-$ and $Bu_3HexN^+TFSI^-$ were chosen for more detailed study because both were liquid at room temperature.

The use of a phosphonium-based IL had several advantages over the analogous ammonium-based IL. The phosphonium IL had higher conductivity and lower viscosity than the ammonium-based IL, which led to higher current densities. The stability of the IL was showed to be dependant on the thermal energy. LiTFSI made little or no contribution to the overall conductivity since its addition caused a decrease in conductivity and increase in viscosity. The decrease in conductivity with addition of a small cation points to a higher degree of ion paring in the present molecules.

Coulombic efficiencies were used to investigate the stability of the deposited metal and were also related to the electrochemical stability of the IL. Lower deposition potentials decreased the coulombic efficiency because at more negative potentials IL

reduction becomes more appreciable. Lower temperatures contributed to higher efficiencies, which may be due to a smaller decrease in lithium ion reduction with temperature than IL reduction. Increasing the LiTFSI concentration also caused an increase in efficiency since more of the cathodic current was used for the reversible deposition of lithium rather than other secondary irreversible processes. At every experimental condition studied, the phosphonium-based IL had a higher coulombic efficiency for lithium electrodeposition and reoxidation than the ammonium-based IL. The bigger size of the phosphonium cation lowers the charge density and the probability of direct nucleophilic attack. Therefore, IL reduction happens at a lower rate than in the ammonium-based IL and this enhances the cycleability of the lithium couple.

Generally, in order to increase the electrochemical stability of a $Quat^+$, higher electron releasing groups (longer alkyl chains) are used, which makes the molecule harder to reduce. However, this increase in stability comes at the expense of lower viscosity due to the added molecular weight and higher probability of entanglement. By changing from an ammonium $Quat^+$ to a phosphonium $Quat^+$ both properties were improved at the same time.

The feasibility of potassium deposition and reoxidation was shown. The addition of a small amount of potassium ions to an IL with lithium ions shifted the reduction potential for the alloy to more positive values giving an increase in the coulombic efficiency compared to lithium alone. Deposition of a lithium-potassium alloy occurred without the formation of dendrites under the conditions where lithium alone formed dendrites. The alloy system could allow for safe use of a lithium metal anode in rechargeable lithium batteries.

5.2 Recommendations for Future Work

There are multiple directions for future work now that improvements in electrolyte and electrode performance have been demonstrated, although two appear to be more promising. First, introduction of other substituents that increase the conductivity and stability of the molecule is of interest to further improve the cycleability of metal deposition. Second, characterization of the alloy deposition in full cell configurations would lead to a better understanding of their practical applicability.

Introduction of an ether linkage has been shown to increase the conductivity and the number of metal ions available for reduction [70]. This could lead to overcoming the low current densities and high viscosities of current systems compared to the organic electrolytes currently used in lithium batteries. Silicon containing groups have also shown to increase the conductivity of the IL [35]. Shrinking the overall size of the cation will also have a similar effect by providing higher conductivities. Introduction of a cyano group inceases the cycling efficiency of lithium metal [56]. Therefore, the impact of the introduction of these groups into the phosphonium cation is of interest since it could increase their potential as practical electrolytes.

The suppression of lithium dendrites should be evaluated as a function of the concentration of the secondary metal (potassium or sodium). Minimizing the quantity of potassium in the electrolyte will keep the specific capacity of the metal anode close to the theoretical value for lithium. The oxide cathode of a battery works on the lithium only cycle; therefore, it is important to minimize the quantity of the secondary metal to a value that avoids its participation in the cathode reaction of the battery but also prevents

dendrite growth. Ideally, the majority of the potassium will reside in the electrolyte during discharge. Therefore the solubility of the metal in the IL is essential. The fact that long dissolution times and high temperatures were needed to dissolve KTFSI in the ILs studied points to its low solubility. Therefore, other metals like sodium could be investigated since a Li-Na alloy has demonstrates to also prevent dendrite growth [22]. After this investigation, full cells could be arranged with an alloy anode and an intercalation cathode and lifetime tests and cycleability performance can be studied. Based on its reversibility, the alloy anode with an IL electrolyte system could result in a reliable and safe secondary battery.

APPENDIX

COULOMBIC EFFICIENCY TABLES

All efficiencies shown were calculated using Method 2

Table A.1 Coulombic efficiencies for $Bu_3HexP^+TFSI^-$ IL with 0.5M LiTFSI

S.P. (V)	Efficiency (%)		
	10°C	25°C	40°C
-1.9	84	74	67
-2.0	77	62	63
-2.1	66	60	48

Table A.2 Coulombic efficiencies for $Bu_3HexP^+TFSI^-$ IL with 1.0M LiTFSI

S.P. (V)	Efficiency (%)	
	10°C	25°C
-1.9	89	77
-2.0	80	67
-2.1	75	63
-2.2	-	59

Table A.3 Coulombic efficiencies for $Bu_3HexP^+TFSI^-$ IL with 1.5M LiTFSI at 25°C

S.P. (V)	Efficiency (%)
-1.9	80
-2.0	69
-2.1	67
-2.2	61
-2.3	58
-2.4	49

Table A.4 Coulombic efficiencies for $Bu_3HexP^+TFSI^-$ IL with 1.5M LiTFSI & 0.075 KTFSI at 25°C

S.P. (V)	Efficiency (%)
-2.0	80
-2.1	78
-2.2	70
-2.3	63
-2.4	57

Table A.5 Coulombic efficiencies for $Bu_3HexN^+TFSI^-$ IL with 0.5M LiTFSI

S.P. (V)	Efficiency (%)		
	10°C	25°C	40°C
-2.0	35	30	28
-2.1	29	23	24
-2.2	21	17	17

Table A.6 Coulombic efficiencies for $Bu_3HexN^+TFSI^-$ IL with 1.0M LiTFSI

S.P. (V)	Efficiency (%)		
	10°C	25°C	40°C
-2.0	69	62	57
-2.1	64	56	50
-2.2	58	50	45

REFERENCES

1. Dollé, M.; Sannier, L.; Beaudoin, B.; Trentin, M. and Tarascon, J., *Electrochemical and Solid State Letters*, **5**, A286 (2002).

2. Brissot, C.; Rosso, M.; Chazalviel, J.; Baudry, P. and Lascaud, S., *Electrochimica Acta*, **43**, 1569 (1998).

3. Brissot, C.; Rosso, M.; Chazalviel, J. and Lascaud, S., *Journal of Power Sources*, **81-82**, 925 (1999).

4. Sakaebe, H., Matsumoto, H. and Tatsumi, K., *Electrochimica Acta*, **53**, 1048-1054 (2007).

5. Seki, S.; Kobayashi, Y.; Miyashiro, H.;, Ohno, Y.; Usami, A.;, Mita, Y.; Kihira, N.; Watanabe, M. and Terada, N., *Journal of Physical Chemistry B*, **110**, 10228-10230 (2006).

6. Gray, G.; J. Winnick and P. Kohl, *Journal of the Electrochemical Society*, **143**, 2262-2266 (1996).

7. Kim, K.; Lang, C. and Kohl, P.A., *Journal of the Electrochemical Society*, **151**, E9-E13 (2005).

8. Seki, S.; Kobayashi, Y.; Miyashiro, H.; Ohno, Y.; Mita, Y.; Usami, A.; Terada, N. and Watanabe, M., *Electrochemical and Solid-State Letters*, **8**, A577-A578 (2005).

9. Matsumoto, H.; Kageyama, H. and Miyazaki, Y. *Chemical Communications*, 1726-1727 (2002).

10. Sun, J.; Forsyth, M. and MacFarlane, D. *Journal of Physical Chemistry B*, **102**, 8858-8864 (1998).

11. Matsumoto, H.; Yanagida, M.; Tanimoto, K.; Nomura, M.; Kitagawa, Y. and Miyazaki, Y., *Chemistry Letters*, 922-923 (2000).

12. Kim, K.; Lang, C. and Kohl, P., *Journal of the Electrochemical Society*, **152**, E56-E60 (2005).

13. Nishida, T.; Tashiro, Y. and Yamamoto, M., *Journal of Fluorine Chemistry*, **120**, 135-141 (2003).
14. Del Sesto, R.; Corley, C.; Robertson, A. and Wilkes, J., *Journal of Organometallic Chemistry*, **690**, 2536-2542 (2005).

15. Bradaric, C.; Downard, A.; Kennedy, C.; Robertson, A. and Zhou, Y., *Green Chemistry*, **5**, 143-152 (2003).

16. Frackowiak, E.; Lota, G. and Pernak, J., *Applied Physics Letters*, **86**, 164104 (2005).

17. Emnet, C.; Weber, K.; Vidal, J.; Consorti, C.; Stuart, A. and Gladysz, J., *Advanced Synthesis and Catalysis*, **348**, 1625-1634 (2006).

18. Ramirez, R. and Sanchez, E., *Solar Energy Materials and Solar Cells*, **90**, 2384-2390 (2006).

19. Tsunashima, K. and Sugiya, M., *Electrochemistry Communications*, **9**, 2353-2358 (2007).

20. Tsunashima, K. and Sugiya, M., *Electrochemical and Solid-State Letters*, **11**, A17-A19 (2008).

21. Besenhard, J.O., *Handbook of Battery Materials*, Wiley-VCH, Weinheim (1999).

22. Doyle, K.; Lang, C.; Kim, K. and Kohl, P., *Journal of the Electrochemical Society*, **153**, A1353 (2006).

23. Despic, A.; Diggle, J. and Bockris, J., *Journal of the Electrochemical Society*, **115**, 507 (1968).

24. Rohnke, M.; Best, T. and Janek, J., *Journal of Solid State Electrochemistry*, **9**, 239 (2005).

25. Zhang, Y. and Abys, A., *Modern Electroplating*, 4th ed., John Wiley and Sons, Inc., New York (2000).

26. Tench, D. and Anderson, D., *Plating and Surface Finishing*, **77**, 44 (1990).

27. Kamitani, M.; Koga, T. and Tsuji, H., *Plating and Surface Finishing*, **72**, 31 (1985).

28. Yoon, S.; Lee, J.; Kim, S. and Sohn, H., *Electrochimica Acta*, **53**, 2501 (2008).

29. Earle, M.; Esperanca, J.; Gilea, M.; Canongia, J.; Rebelo, L.; Magee, J.; Seddon, K. and Widegren, J., *Nature*, **439**, 831-834 (2006).

30. Paulechka, Y.; Zaitsau, D.; Kabo, G. and Strechan, A., *Thermochimica Acta*, **439**, 158-160 (2005).

31. Robinson, J. and Osteryoung, R., *Journal of the American Chemical Society*, **101**, 323-327 (1979).

32. Cheek, G. and Osteryoung, R., *Inorganic Chemistry*, **21**, 3581-3584 (1982).

33. Wilkes, J.; Levisky, J.; Wilson, R. and Hussey, C., *Inorganic Chemistry*, **21**, 1263-1264 (1982).

34. Gifford, P. and Palmisano, J., *Journal of the Electrochemical Society*, **134**, 610-614 (1987).

35. Shirota, H. and Castner, E., *Journal of Physical Chemistry B*, **109**, 21576-21585 (2005).

36. Bonhote, P.; Dias, A.; Papageorgiou, N.; Kalyanasundaram, K. and Gratzel, M., *Inorganic Chemistry*, **35**, 1168-1178 (1996).

37. Zhou, Z.; Matsumoto, H. and Tatsumi, K., *Chemistry: A European Journal*, 10, 6581-6591 (2004).

38. Zhou, Z.; Matsumoto, H. and Tatsumi, K., *Chemistry: A European Journal*, **11**, 752-766 (2005).

39. Matsumoto, H.; Sakaebe, H. and Tatsumi, K. *Journal of Power Sources*, **146**, 45-50 (2005).

40. Zhao, D.; Fei, Z.; Scopelliti, R. and Dyson, P., *Inorganic Chemistry*, **43**, 2197-2205 (2004).

41. Wilkes, J. and Zaworotko, M., *Journal of the Chemical Society-Chemical Communications*, 965-967 (1992).

42. Fuller, J.; Carlin, R.; Delong, H. and Haworth, D., *Journal of the Chemical Society-Chemical Communications*, 299-300 (1994).

43. McFarlane, D.; Sun, J.; Golding, J.; Meakin, P. and Forsyth, M. *Electrochimica Acta*, **45**, 1271-1278 (2000).

44. Zhou, Z.; Matsumoto, H. and Tatsumi, K. *Chemistry Letters*, **33**, 1636-1637 (2004).

45. Yu, C.; Winnick, J. and Kohl, P. *Journal of the Electrochemical Society*, **138**, 339-340 (1991).

46. Scordilis-Kelley, C.; Fuller, J.; Carlin, R. and Wilkes, J. *Journal of the Electrochemical Society*, **139**, 694-699 (1992).

47. Riechel, T. and Wilkes, J. *Journal of the Electrochemical Society*, **139**, 977-981 (1992).

48. Scordilis-Kelley, C. and Carlin, R. *Journal of the Electrochemical Society*, **140**, 1606-1611 (1993).

49. Gray, G.; Kohl, P. and Winnick, J. *Journal of the Electrochemical Society*, **142**, 3636-3642 (1995).

50. Fuller, J.; Osteryoung, R. and Carlin, R. *Journal of the Electrochemical Society*, **142**, 3632-3636 (1995).

51. Fung, Y. and Zhou, R., *Journal of Power Sources*, **81/82**, 891-895 (1999).

52. Sakaebe, H. and Matsumoto, H., Electrochemistry Communications, 5, 594-598 (2003).

53. Zheng, H.; Li, B.; Fu, Y.; Abe, T. and Ogumi, Z., *Electrochimica Acta*, **52**, 1556-1562 (2006).

54. Hu, Y.; Li, H. and Huand, X., *Electrochemistry Communications*, **6**, 28-32 (2004).

55. Garcia, B.; Lavalee, S.; Perron, G.; Michot, C. and Armand, M., *Electrochimica Acta*, **49**, 4583-4588 (2004).

56. Egashira, M.; Okada, S.; Yamaki, J.; Dri, A.; Bonadies, F. and Scrosati, B., *Journal of Power Sources*, **138**, 240-244 (2004).

57. Egashira, M; Nakagawa, M.; Watanabe, I.; Okada, S. and Yamaki, J., *Journal of Power Sources*, **146**, 685-688 (2005).

58. Wasserscheid, P. and Keim, W. *Angewandte Chemie, International Edition*, **39**, 3772 (2000).

59. Welton, T. *Chemical Reviews (Washington, D. C.)*, **99**, 2071 (1999).

60. Park, S.; Kazlauskas, R. J. *Current Opinion in Biotechnology*, **14**, 432-437 (2003).

61. Navarra, M.; Panero, S. and Scrosati, B. *Electrochemical and Solid State Letters*, **8**, A324-A327 (2005).

62. Lu, W.; Fadeev, G.; Qi, B.; Smela, E.; Mattes, B.; Ding, J.; Spinks, G.; Mazurkiewicz, J.; Zhou, D.; Wallace, G.; MacFarlane, D.; Forsyth, S. and Forsyth, M., *Science (Washington, DC, United States)*, **297**, 983 (2002).

63. Matsumoto, H.; Matsuda, T.; Tsuda, T.; Hagiwara, R.; Ito, Y. and Miyazaki, Y. *Chemistry Letters*, **30**, 26-27 (2001).

64. Wang, P.; Zakeeruddin, S. M.; Comte, P.; Exnar, I. and Graetzel, M. *Journal of the American Chemical Society*, **125**, 1166-1167 (2003).

65. Sato, T.; Masuda, G. and Takagi, K. *Electrochimica Acta*, **49**, 3603-3611 (2004).

66. Wen, S.; Richardson, T.; Ghantous, D.; Striebel, K.; Ross, P. and Cairns, E., *Journal of Electroanalytical Chemistry*, **408**, 113-118 (1996).

67. Henderson W. and Buckler, S., *Journal of the American Chemical Society*, **82**, 5794-5800 (1960).

68. Lang, C.; Kim, K.; Guerra, L. and Kohl, P., *Jounal of Physical Chemistry B*, **109**, 19454-19462 (2005).

69. Howlett, P.; MacFarlane, D. and Hollenkamp, A., *Electrochemical and Solid-State Letters*, **7**, A97-A101 (2004).

70. Lang, C. and Kohl, P., *Journal of the Electrochemical Society*, **154**, F106-F110 (2007).